Amplified Drought and Flood Risk Under Future Socioeconomic and Climatic Change

Tabari, Hossein; Hosseinzadehtalaei, Parisa; Thiery, Wim; Willems, Patrick

Published in:
Earth's Future

DOI:
10.1029/2021EF002295

Publication date:
2021

Earth's Future

RESEARCH ARTICLE
10.1029/2021EF002295

Key Points:

- A large increase in flood and drought risk is projected towards the end of the century over most of the global land area
- Shifting from a fossil-fueled development to a sustainable one reduces both flood and drought risk by half
- South America and Africa are identified as risk hotspots

Supporting Information:

Supporting Information may be found in the online version of this article.

Correspondence to:

H. Tabari,
hossein.tabari@kuleuven.be

Citation:

Tabari, H., Hosseinzadehtalaei, P., Thiery, W., & Willems, P. (2021). Amplified drought and flood risk under future socioeconomic and climatic change. *Earth's Future*, 9, e2021EF002295. https://doi.org/10.1029/2021EF002295

Received 30 JUN 2021
Accepted 29 SEP 2021

Author Contributions:

Conceptualization: Hossein Tabari
Data curation: Hossein Tabari
Formal analysis: Hossein Tabari, Parisa Hosseinzadehtalaei
Funding acquisition: Hossein Tabari
Investigation: Hossein Tabari
Methodology: Hossein Tabari, Parisa Hosseinzadehtalaei
Resources: Hossein Tabari
Visualization: Hossein Tabari
Writing – original draft: Hossein Tabari
Writing – review & editing: Hossein Tabari, Parisa Hosseinzadehtalaei, Wim Thiery, Patrick Willems

Amplified Drought and Flood Risk Under Future Socioeconomic and Climatic Change

Hossein Tabari[1], Parisa Hosseinzadehtalaei[1], Wim Thiery[2], and Patrick Willems[1,2]

[1]Department of Civil Engineering, KU Leuven, Leuven, Belgium, [2]Department of Hydrology and Hydraulic Engineering, Vrije Universiteit Brussel, Brussels, Belgium

Abstract The economic stress and damage from natural hazards are escalating at an alarming rate, calling for anticipatory risk management. Yet few studies have projected flood and drought risk, owing to large uncertainties, strong non-linearities, and complex spatial-temporal dynamics. Here, we develop an integrative global risk analysis framework encapsulating future changes in flood and drought hazards as well as associated exposure and vulnerability dimensions. Flood characteristics are quantified by fitting a generalized extreme value distribution (GEV) to the annual flow maxima time series, while drought properties are characterized by the standardized precipitation evapotranspiration index (SPEI) and the standardized precipitation index (SPI). The drivers of drought and flood risk changes at the global and regional scales are explored, and the wide cascade of uncertainties in the risk assessment is decomposed. We find a substantial increase in both flood and drought risk towards the end of the century over most of the globe, driven by compounding changes in exposure, vulnerability, and hazard. A shift from a fossil-fueled development to a sustainable one decreases the global area facing a risk doubling from 61% to 33% for flood and from 41% to 23% for drought. South America and Africa are identified as hotspot regions where a concomitant, large increase in both flood and drought risk are projected. The hazard quantification method is ubiquitously the dominant uncertainty source for drought risk changes, while the contribution of uncertainty sources for flood risk changes is highly variable in space.

Plain Language Summary The number of natural hazards has accelerated sharply in the past few decades, with hydrology-related catastrophes being responsible for >50% of the total fatalities. The risk of extreme events thus warrants investigation in order to formulate efficient adaptation and risk management policies. Here, we scrutinize changes in flood and drought risk over the global land area for the end-21st-century to identify leverage points in reducing the risk. Our results show an increase in both flood and drought risks over most of the area. South America and Africa are identified as hotspot regions where a concurrent, large increase in both flood and drought risks are projected, necessitating integrated policies and practices for deliberate and effective disaster risk reduction in these regions. Our findings provide a basis for better decision-making to curb the growing impacts of the extremes and socioeconomic developments.

1. Introduction

Natural hazards have caused over 1.6 million fatalities worldwide since 1990 and resulted in an annual economic loss of about $260–310 billion (Ward, Blahut, et al., 2020). Over 50% of the economic losses from natural disasters are ascribed to floods and droughts. Flooding caused about 43% of natural disasters over the last 20 years and affected nearly 2.5 billion people globally, while drought with just 5% share of the total disasters affected 25% of the global total population (CRED, 2015). The economic stress and damage from natural hazards are on the rise at an alarming rate, and 2018 was the fourth-costliest year in history. With risk being defined as a function of three components including hazard, exposure, and vulnerability (Cardona et al., 2012), the increasing risk of natural hazards is driven by an amplified frequency, duration, and intensity of hazards due to climate change (IPCC, 2013; Ahmadalipour et al., 2019; Hosseinzadehtalaei et al., 2020) as well as an increased human and infrastructure settlement and activities in areas exposed to these hazards (Kam et al., 2021; Khajehei et al., 2020; Knorr et al., 2016).

The urgency to mitigate the significant risk of natural hazards and to create resilient, future-proof infrastructure has been recognized by international scientific and policy communities and have become the

core of the Sendai Framework for Disaster Risk Reduction (UNISDR, 2015) and the Warsaw International Mechanism for Loss and Damage Associated with Climate Change Impacts (UNFCCC, 2013). In this context, deliberate disaster risk reduction (DRR) efforts and effective adaptation strategies aim at lowering the magnitude of each of the three risk components (UNISDR, 2013; Alfieri et al., 2016). Although the focus to date for risk reduction has been more on reducing the occurrence probability of hazards through extensive structural defense systems, nonstructural actions such as reducing the exposure of people, economies, and ecosystems to hazards and reducing the vulnerability of those exposed to hazards have increasingly been implemented in recent years.

In previous global flood risk studies, vulnerability has been considered by using a limited number of proxy indicators. This is partly due to the limited availability of future gridded socioeconomic data at the global scale, while a wide range of indicators is available at the local and regional scales to determine flood or drought vulnerability (Engström et al., 2020; Kim et al., 2015; Nasiri et al., 2016; Scheuer et al., 2011). Most global flood studies to date have solely considered future population exposure and economic vulnerability as expressed by gross domestic product (GDP) (Hinkel et al., 2014; Jongman et al., 2015; Kinoshita et al., 2018; Liao et al., 2019; Tanoue et al., 2016; Vafeidis et al., 2019; Ward et al., 2017). Yet GDP alone is a poor proxy of vulnerability because the vulnerability of communities and/or people can be very large even in rich countries, as exemplified by the summer 2003 European heatwave with a total of 68,312 fatalities (Formetta and Feyen, 2019). Other studies have projected changes in global flood risk using static exposure and/or vulnerability and dynamic hazards (Alfieri et al., 2017; Hirabayashi et al., 2013; Lange et al., 2020; Willner et al., 2018). Proper attention to the dynamic nature of exposure and vulnerability is, however, extremely important considering that the design and implementation of risk management and adaptation policies may lead to a risk probability decrease in short-term, but an increase over longer-term (Cardona et al., 2012). In this context, the future risk increase of some extreme events was found to be driven by future population expansion in hazard-prone regions rather than hazard intensification (Knorr et al., 2016). Apart from the population exposure and economic vulnerability, additional dimensions of flood vulnerability such as urbanization and agricultural value have been investigated in a handful future (Dottori et al., 2018; Jongman et al., 2012; Vousdoukas et al., 2018, 2020; Winsemius et al., 2013, 2016) and historical (Ward et al., 2013) flood risk assessments.

For future drought risk, a relatively larger number of global studies have been carried out using a broad variety of approaches and indicators. Nevertheless, previous drought risk assessments mostly considered historical hazard, exposure, and vulnerability (Carrão et al., 2016; Meza et al., 2020), dynamic future hazards under static exposure and/or vulnerability (Gu et al., 2020; Lange et al., 2020; Li et al., 2009; Pokhrel et al., 2021) and dynamic hazards with only a dynamic exposure (Arnell et al., 2018; Gu et al., 2020; Liu et al., 2018; Smirnov et al., 2016). Yet none of the previous studies have considered dynamic hazard, exposure, and vulnerability for future risk assessments of global droughts.

The knowledge gaps in drought and flood risk assessments demonstrate the need to develop an integrated global vulnerability and risk framework to capture a greater range of dimensions and factors of vulnerability and disaster risk (e.g., social, cultural, economic, physical, and environmental aspects), the nonlinear relations of the factors and the dynamics of the vulnerability and risk. The limited dimensions of vulnerability used in previous studies may constitute a serious limitation in global risk estimates. The importance of integrating different vulnerability indicators was particularly emphasized for future climate change impact assessments, e.g., combining three indicators of national-scale education level, the gender gap in education, and GDP to characterize the quality and efficiency of governance for climate change adaptation (Andrijevic et al., 2020).

Risk analysis also involves several methods which introduce uncertainty to the analysis results, such as climate modeling, hydrological modeling, and hazard and vulnerability assessments (Hosseinzadehtalaei et al., 2020). The uncertainty quantification in the field of risk assessment, however, remains largely underdeveloped, despite important information it provides for a better interpretation of climate change impacts as well as for informed policies to mitigate the associated risk (Webster et al., 2003). Furthermore, the relative importance of exposure, vulnerability, and hazard in projected flood and drought risk has rarely been quantified.

In this study, we provide a comprehensive assessment of the risk changes for both flood and drought globally. To this end, an integrative global framework is developed to combine changes in different flood and drought characteristics and in different exposure and vulnerability components. We define the risk as the multiplication of the hazards and exposure-vulnerability metrics. Three scenario combinations for future risk assessments are considered: "Sustainability" (shared socioeconomic pathway (SSP) SSP1 combined with representative concentration pathway (RCP) RCP2.6), "Regional rivalry" (SSP3 combined with RCP6.0), and "Fossil-fueled development" (SSP5 combined with RCP8.5). The Sustainability and Fossil-fueled development scenarios both envision a world with a relatively high income growth, rapid urbanization, and higher investments in health and education. While in the former this relatively optimistic trend for future economic and social developments is obtained by an increasing shift towards sustainable practices, it is achievable by an energy-intensive, fossil fuel-based economy in the latter. The Regional rivalry scenario describes pessimistic human development with a lack of investments in education and health, a fast-growing population, and more inequality (O'Neill et al., 2016).

We develop a composite exposure and vulnerability index by consolidating changes in social, economic, and physical proxy indicators. Because the future gridded socioeconomic data relevant for flood and drought vulnerability are only available for population, GDP, and land use, they are used here to derive the indicators. Flood and drought hazard indices are also established by integrating changes in intensity, duration, and frequency of the hazards. Our framework provides a comprehensive risk assessment given that disregarding any of the determinants of exposure, vulnerability, and hazard components may lead to an underestimation of the risk. For instance, a drought of moderate severity but with a long duration is hardly recognized as an extreme event, while it may lead to large socioeconomic losses due to its potential to rapidly deplete stored water and thereby diminish resilience to following droughts (Lehner et al., 2017). This issue is efficiently addressed in our hazard index which combines changes in different characteristics.

We characterize drought properties by the standardized precipitation evapotranspiration index (SPEI) and the standardized precipitation index (SPI) using simulations of 18 global climate models (GCMs) from the Coupled Model Intercomparison Project Phase 5 (CMIP5), (Taylor et al., 2012) under RCP2.6, RCP6.0, and RCP8.5 scenarios. Flood characteristics are quantified by fitting a generalized extreme value distribution (GEV) to the annual flow maxima time series from 84 realizations (seven global hydrological models, GHM, fed by four CMIP5 GCMs under RCP2.6, RCP6.0, and RCP8.5) from phase 2b of the Inter-Sectoral Impact Model Intercomparison Project (ISIMIP2b; Frieler et al., 2017). The drivers of drought and flood risk changes at the global and regional scales are explored by analyzing the changes in the hazard and exposure-vulnerability components. Finally, the wide cascade of uncertainties in the risk assessment is decomposed at the regional scale.

2. Materials and Methods

2.1. Data

For the drought risk assessment, we analyze monthly precipitation, maximum, minimum and mean air temperature simulations from 18 GCMs participating in CMIP5 (Table S1 in Supporting Information S1). The 18 models were chosen based on their data availability. To allow all multi-model ensemble members to receive equal weight in ensemble median (i.e., unweighted median), only the first realization (r1) of each model is considered. The selected historical period is from 1971 to 2000 and the future period from 2070 to 2099 forced by three representative concentration pathways (RCPs), (Van Vuuren et al., 2011) 2.6, 6.0, and 8.5. These pathways refer to a stringent mitigation scenario resulting in low radiative forcing levels (RCP2.6), a medium-high scenario (RCP6.0), and a high-end emission scenario (RCP8.5). Although the drought risk analysis may have limited practical implications for deserts and hyper-arid regions, it may provide useful information for a physical understanding of climate change impact in these regions. The drought risk analysis is hence performed on the entire global land area as opposed to some studies which excluded deserts and hyper-arid regions (Carrão et al., 2016; Naumann et al., 2018).

We also analyze daily discharge simulations from seven ISIMIP global hydrological models (GHMs) forced by climate projections from four CMIP5 GCMs (GFDL-ESM2M, HadGEM2-ES, IPSL-CM5A-LR, and MIROC5) for climate change impact assessment on flooding. The GHMs are CLM4.5 (Lawrence et al., 2011;

Thiery et al., 2017), H08 (Hanasaki et al., 2008), JULES-W1 (Best et al., 2011), LPJmL (Bondeau et al., 2007), MATSIRO (Takata et al., 2003), ORCHIDEE (Guimberteau et al., 2014), and WaterGAP2 (Mueller Schmied et al., 2016). A comprehensive overview of the modeling frameworks of these GHMs is provided by Telteu et al. (2021). We consider the same historical and future periods and concentration pathways as the CMIP5 simulations for the ISIMIP2b simulations. Model grid cells with annual flow maxima of <1 m^3 s^{-1} of the historical period are excluded for further analysis, because of the smaller importance for flood analysis and inadequate data for distribution fitting. The Southern Hemisphere high-latitude landmass (>60°S) is also screened out as it is almost uninhabited and not subject to flooding.

The annual population density, urbanized areas, and GDP data on a 0.5° × 0.5° grid available through ISIMIP for the historical (1971–2000) and future (2070–2099) periods are used. The annual country-level GDP data were downscaled to 0.5° grid resolution based on the methodology described in Murakami and Yamagata (2019). Historical population density and urbanized areas data are based on the HYDE3.2 database (Klein Goldewijk et al., 2017). Future population data are derived from the national population projections based on the shared socioeconomic pathways (SSPs), (O'Neill et al., 2014) SSP1, SSP3, and SSP5 as described in Samir and Lutz (2014). The future urbanization patterns are based on the projections from the MAgPIE land-use model (Popp et al., 2014; Stevanovic et al., 2016) according to SSP2 and RCP2.6 and RCP6.0. To make a smooth transition between the historical (HYDE3.2) and future land-use patterns, a harmonization algorithm was applied to the MAgPIE data. We use the gridded land use data on a 0.5° × 0.5° grid from AIM-SSP/RCP Gridded Emissions and Land-use data set (Fujimori et al., 2018) to obtain the proportion of total croplands. The cropland proportion data for three combinations of SSP1-RCP2.6, SSP3-RCP6.0, and SSP5-RCP6.0 are utilized (SSP5-RCP8.5 combination is not available).

2.2. Assessment of Risk Changes

The change in the risk of drought and flood is calculated for each model grid cell by multiplying the change rate of hazard and exposure-vulnerability using Equation 1.

$$\delta_{\mathrm{DR}}(g) = \delta_{\mathrm{DHI}}(g) \times \delta_{\mathrm{CEVI}}(g) \tag{1a}$$

$$\delta_{\mathrm{FR}}(g) = \delta_{\mathrm{FHI}}(g) \times \delta_{\mathrm{CEVI}}(g) \tag{1b}$$

In which,

$$\delta_{\mathrm{DHI}}(g) = \frac{\mathrm{DHI}_f(g)}{\mathrm{DHI}_h(g)} \tag{2a}$$

$$\delta_{\mathrm{FHI}}(g) = \frac{\mathrm{FHI}_f(g)}{\mathrm{FHI}_h(g)} \tag{2b}$$

$$\delta_{\mathrm{CEVI}}(g) = \frac{\mathrm{Pop}_f(g)}{\mathrm{Pop}_h(g)} \times \frac{Ur_f(g)}{Ur_h(g)} \times \frac{\mathrm{GDP}_h(g)}{\mathrm{GDP}_f(g)} \times \frac{Cr_f(g)}{Cr_h(g)} \tag{3}$$

where at each grid cell g for future (f) and historical (h) periods, δ_{DR}, δ_{FR}, δ_{DHI}, δ_{FHI}, and δ_{CEVI} are the relative changes between the future (2070–2099) and historical (1971–2000) periods for drought risk (DR), flood risk (*FR*), drought hazard index (DHI), flood hazard index (FHI) and composite exposure-vulnerability index (CEVI), respectively, Pop is the total population density, GDP is the gross domestic product per capita and *Ur* and *Cr* are proportions of urbanization and croplands, respectively. The relative change in GDP is inverted due to its indirect relation with vulnerability. The DHI and FHI will be defined in the following section. To avoid having zero values in the multiplicative approach of the CEVI quantification, the proxy indicators are normalized between 0.05 and 0.95 for historical and future periods separately. Due to the limited relevance of urbanization for drought risk, it is not considered for the drought CEVI. The risk assessment is performed under three combined scenarios: "Sustainability" (SSP1 combined with RCP2.6), "Regional rivalry" (SSP3 combined with RCP6.0), and "Fossil-fueled development" (SSP5 combined with RCP8.5).

2.3. Hazard Quantification Procedure

The change in the drought hazard index for each grid cell ($\delta_{\mathrm{DHI}}(g)$) is computed as the multiplicative combination of the change in three drought properties of intensity, frequency, and duration. Equation 2a can then be written as follows (Equation 4):

$$\delta_{\mathrm{DHI}}(g) = \frac{I_f(g)}{I_h(g)} \times \frac{F_f(g)}{F_h(g)} \times \frac{D_h(g)}{D_f(g)} \tag{4}$$

where at each grid cell g for future (f) and historical (h) periods, I, F, and D are drought intensity, frequency, and duration, respectively. We use an equal weight for the three properties as they are considered equally important in generating the hazardous impact of drought (Maccioni et al., 2015).

To characterize drought, we compute the time series of the Standardized Precipitation Evapotranspiration Index (SPEI), (Vicente-Serrano et al., 2010) values for each grid cell and each GCM. SPEI uses the difference between precipitation and evapotranspiration as a measure of drought or sustainable water availability, better characterizes the occurrence of dryer conditions and considers the impact of global warming (Peña-Gallardo et al., 2019). Evapotranspiration is calculated by the Hargreaves-Samani method (Hargreaves and Samani, 1985) that effectually incorporates solar radiation by its indirect approximation from maximum and minimum temperatures.

To explore the influence of excluding air temperature for the drought characterization, drought is also quantified using the standardized precipitation index (SPI), (McKee et al., 1993), which is the most frequently used index for drought characterization (Alborzi et al., 2018; Chiang et al., 2018; Hirschi et al., 2011; Tabari et al., 2012), also recommended by the World Meteorological Organization (WMO, 2012) and the National Drought Mitigation Center (NDMC, 2018). The empirical probabilities of precipitation for SPI and precipitation-evapotranspiration difference for SPEI are computed to avoid any assumption on the underlying distribution function of the data (Farahmand and AghaKouchak, 2015). The difference between the SPEI and SPI results is analyzed in terms of hazard quantification uncertainty in the uncertainty decomposition of future drought risk. The Wilcoxon rank-sum test is also used for testing the statistical significance of the difference.

To account for annual drought patterns, a 12-month accumulation period is used which represents anomalies of accumulated precipitation or precipitation-evapotranspiration difference for the given month and the 11 previous months. This is the time scale of the globally most extreme drought events in the last decades (Sheffield and Wood, 2011) and was shown to have the best predictive ability of the likelihood of impact occurrence in different sectors (Blauhut et al., 2016). Similar to Spinoni et al. (2020), we select the entire period (1971–2099) as a baseline period to compute the anomalies in the SPI and SPEI methods. Using a longer baseline period ensures a more robust characterization of standardized drought indicators (Wu et al., 2005), as the selection of a shorter period with a different drought frequency and severity may affect the indicator values over the entire period, resulting in underestimation or overestimation of climate change impact on drought. Furthermore, using past data as a baseline period to explore future drought events may introduce bias in calculated climate change signals, as normal conditions in the past will change in the future, leading to unrealistically extreme events at the end of the twenty-first century.

We derive the drought characteristics (i.e., drought duration, frequency, and intensity) using the run theory where a run represents a part of time series wherein drought index is either below (negative run) or over (positive run) a given drought defining threshold. In the current study, a drought event occurs every time the SPI/SPEI indicator falls below −1 for at least two consecutive months, and it ends when the indicator rises above zero (McKee et al., 1993). The drought threshold of −1 corresponds to the higher limit of a moderate drought. Drought in this study, therefore, includes moderate ($-1.5 < \mathrm{SPI/SPEI} < -1$), severe ($-2 < \mathrm{SPI/SPEI} < -1.5$), and extreme ($\mathrm{SPI/SPEI} < -2$) droughts. The drought frequency is defined as the number of drought events for the historical (1971–2000) and future (2070–2099) periods. The duration of a drought event refers to the number of months between its start and end month. The drought intensity (dimensionless) is the average indicator value of a drought event. For each GCM, we calculate drought frequency and the medians of drought duration and intensity across all drought events at each grid cell for historical and future periods. The ratio of the magnitude of drought characteristics in the future period over that of the corresponding characteristics in the historical period is then used in Equation 4. To compute the

ensemble median, the CMIP5 GCMs with different horizontal resolutions are resampled from their native scale to a 0.5° (latitude) ×0.5° (longitude) grid. We use the last-step procedure for the resampling where climate change signals are calculated directly on the native grids of GCMs, and then resampled. The error of the last-step procedure is less than the first-step procedure in which precipitation is first resampled, and then climate change signals are computed (Diaconescu et al., 2015).

Similar to DHI, the change in flood hazard index (FHI) for each grid cell ($\delta_{\mathrm{FHI}}(g)$) is calculated as the multiplicative combination of the change rate of flood intensity and frequency using Equation 5. Note that the change in flood duration cannot be determined using the available data. Equation 2b can accordingly be written as follows (Equation 5):

$$\delta_{\mathrm{FHI}}(g) = \frac{I_f(g)}{I_h(g)} \times \frac{F_f(g)}{F_h(g)} = \frac{I_f(g)}{I_h(g)} \times \frac{T_h(g)}{T_f(g)} \tag{5}$$

The notations have the same meaning as before. The change in flood frequency is computed as the change in the return period (T). Because an increase in the return period means a decrease in frequency and vise versa, the relative change in return period is reversed in Equation 5 to obtain the change in flood frequency.

To exclude the possible extrapolation bias in estimating flow quantiles from the 30-year data (1971–2000 and 2070–2099) and to enable a direct comparison with similar studies (e.g., Arnell et al., 2018; Dankers et al., 2014), the river flow with a 30-year return period (average occurrence of once every 30 years) at each model grid cell is used as a proxy for flooding. To this end, a generalized extreme value distribution (GEV) is fitted to the annual flow maxima time series for each native grid cell of the GHMs for both historical and future periods (Tabari, 2021). The river flow intensity associated with the return period T is subsequently computed by:

$$I_T = \begin{cases} \mu + \dfrac{\sigma}{\xi}\left\{1 - \left[-\ln\left(1 - \dfrac{1}{T}\right)\right]^{\xi}\right\} & if \quad \xi \neq 0 \\ \mu - \sigma ln\left[-\ln\left(1 - \dfrac{1}{T}\right)\right] & if \quad \xi = 0 \end{cases} \tag{6}$$

where I_T is the river flow for return period T (30 in our case), and μ, σ, and ξ are the location, scale, and shape parameters of the GEV distribution. The ratio of the flood intensity of a 30-year return period between future and historical periods is utilized in Equation 5 as the change in flood intensity.

To calculate the frequency of flood events, the future return period of the historical extreme flow of $T = 30$ years is derived from Equation 7.

$$T = \frac{1}{1 - \psi(I_T)} \tag{7}$$

where $\psi(I_T)$ is given in Equation 8:

$$\psi(I_T) = \exp\left\{-\left[1 + \xi\left(\frac{I_T - \mu}{\sigma}\right)\right]^{-\frac{1}{\xi}}\right\} \tag{8}$$

where ψ is defined for $1 + \xi\left(\dfrac{I_T - \mu}{\sigma}\right) > 0$, elsewhere ψ is either 0 or 1. The historical return period (30 in this study) is divided over the obtained future return period in Equation 5 as the change factor in flood frequency.

2.4. Decomposing the Cascade of Uncertainties

We partition the cascade of uncertainties in flood and drought risk changes at a regional scale following the variance decomposition-same sample size (VD-SSS) method (Tabari et al., 2019) as traditional VD methods (Greve et al., 2018) artificially inflates uncertainty contributions from sources with larger sample sizes (Hosseinzadehtalaei et al., 2017). The total uncertainty in the projections of future flood and drought risk is partitioned into contributions from climate model response (GCM uncertainty), global hydrological models

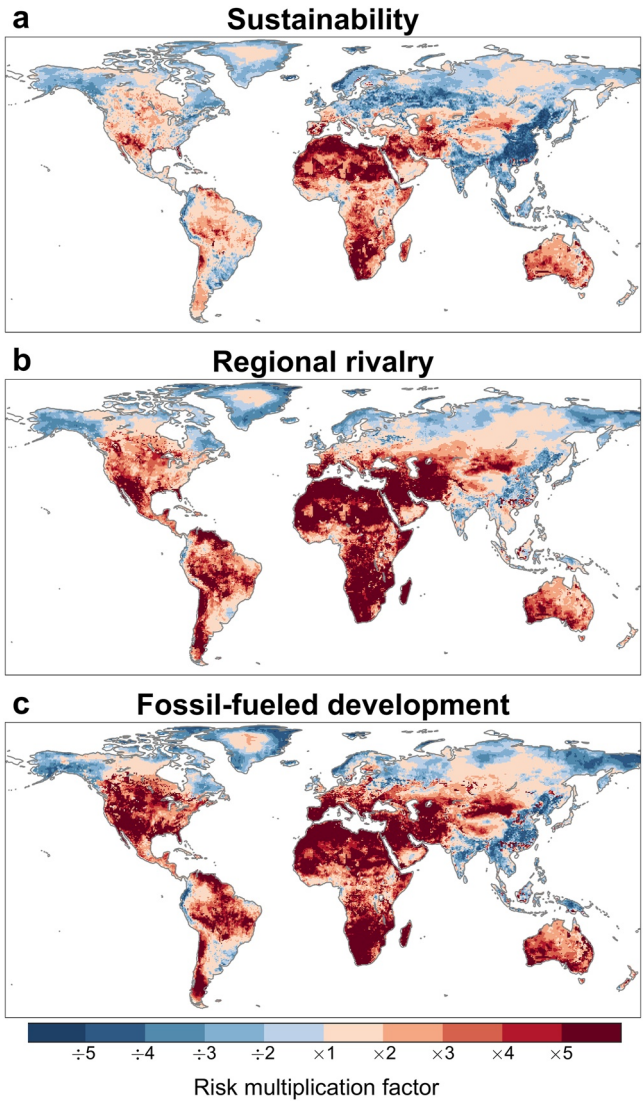

Figure 1. Global patterns of change in drought risk by 2070–2099 under (a) Sustainability, (b) Regional rivalry, and (c) Fossil-fueled development scenarios relative to 1971–2000. The changes are based on the ensemble median of 18 CMIP5 GCMs.

for flood and the multi-scaler indices for drought (hazard quantification uncertainty), emission scenarios for the future hazard projections (RCP uncertainty), and SSP scenarios for the future CEVI projections (SSP uncertainty).

In the iterative sampling-theory based bootstrapping procedure of VD-SSS, let n denotes the smallest sample size among the uncertainty components (3 for flood risk and 2 for drought risk) and N be the ensemble size. After taking the median across the other uncertainty components, n is randomly drawn from N and the standard deviation across the bootstrap samples is calculated. This process is repeated many times (1,000 iterations in our case) and the median of the empirical bootstrap distribution of sample standard deviation signifies the uncertainty. The traditional VD method is applied for the uncertainty component of size n (here, hazard quantification uncertainty for drought and RCP and SSP uncertainties for flood). The fractional uncertainties are defined as the uncertainty of each source divided by the total uncertainty and the total uncertainty equals the sum of the uncertainty contributions (Tabari et al., 2019).

3. Results

3.1. Projected Changes in Drought Risk

The global map of the future changes in drought risk based on the multi-model ensemble median shows strong increases (>threefold) in the risk by the end of the 21st century in most of South America, the Caribbean, central America, the United States, southern Europe, Middle East and North Africa (MENA), southern Africa, and Australia (Figure 1). Projected drought risk decreases in the rest of the global land area, mainly in the Russian Federation, northern Europe, southern Alaska, and Canada, but also parts of South America, and eastern and southeastern Asia. Of the global land grid cells, 50%, 62%, and 61% show an increase in the drought risk under the Sustainability, Regional rivalry, and Fossil-fueled development scenarios, respectively. For the respective scenarios, the drought risk is projected to at least double in 23%, 39%, and 41% of the global landmass and at least triple in 13%, 28%, and 31% of the area. As expected, the area experiencing an increased drought risk increases with rising GHG emissions and socioeconomic developments.

To further quantify the spatial distribution of the risk changes, the changes are analyzed for 21 continental and subcontinental land regions (Giorgi and Francisco, 2000) (Figure S1 in Supporting Information S1). The drought risk is expected to increase in 13, 17, and 16 regions under the Sustainability, Regional rivalry, and Fossil-fueled development scenarios, respectively (Figure 2a). The projected changes in the drought risk increase from the Sustainability to the Fossil-fueled development scenario, with drought risk tripling in 2, 5, and 7 regions under the Sustainability, Regional rivalry, and Fossil-fueled development scenarios, respectively. Apart from the Sahara region, the highest increases in the drought risk are found in southern Africa, the Mediterranean basin, central Asia, and central North America where the future risk is more than five times larger than the historical risk under the Fossil-fueled development scenario. In these regions, 100% of the area experience a drought risk increase under the Regional rivalry and Fossil-fueled development scenarios, while for the Sustainability scenario 83%, 89%, 91%, and 100% of the area of central Asia, central North America, Mediterranean basin, and southern Africa face a drought risk increase (Figure 3). Apart from the area under risk, an increasing trend magnitude of the risk changes with GHG emissions and socioeconomic developments is also evident for all the regions (Figure 2a). In the four hotspot regions, the risk change under the Fossil-fueled development scenario is 2–2.7 times larger than that under the Sustainability scenario (Figure 3).

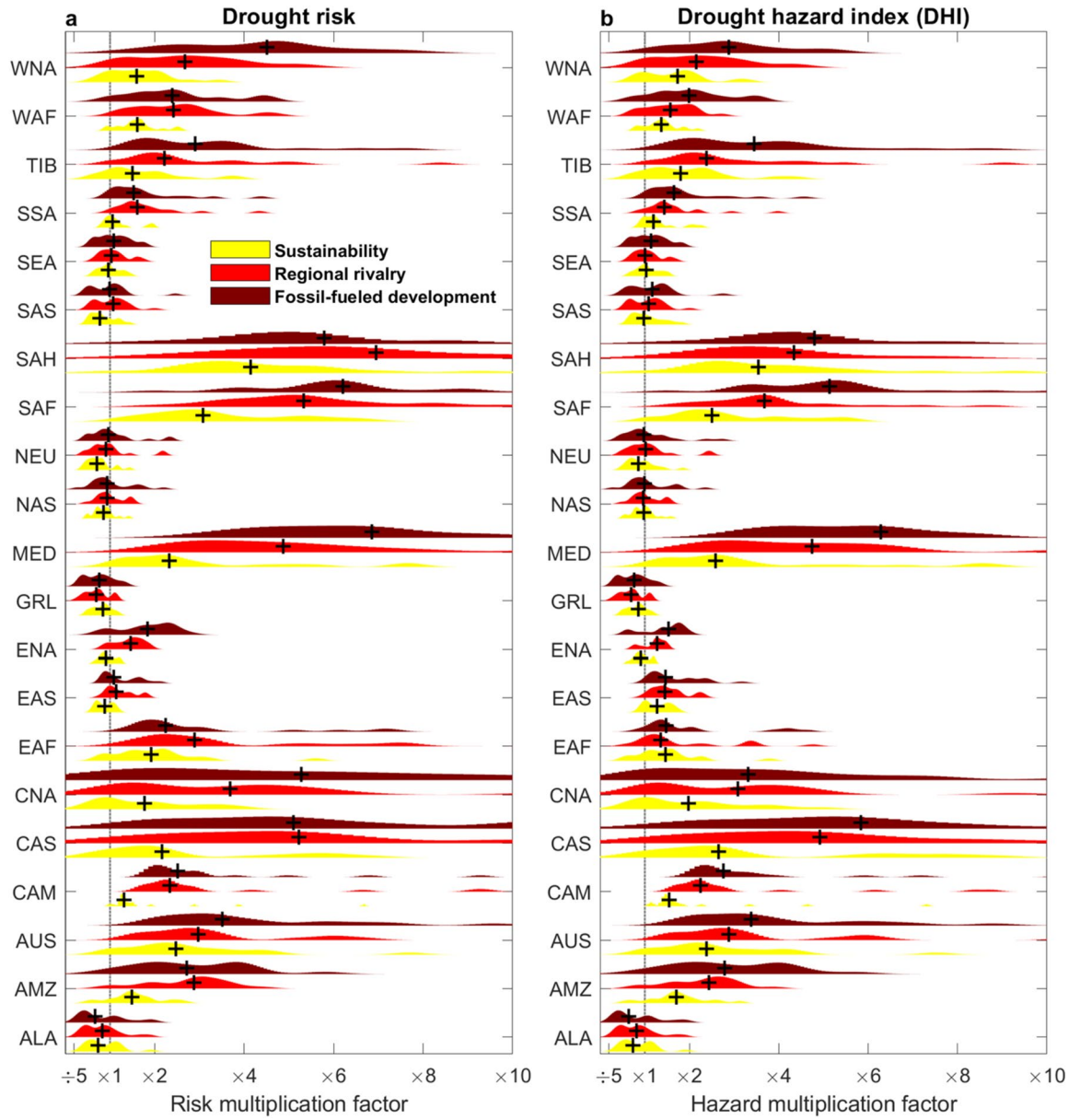

Figure 2. Change in (a) drought risk and (b) drought hazard index (DHI) in 21 continental and subcontinental regions by 2070–2099 relative to 1971–2000. See Table S2 in Supporting Information S1 for the full names of the abbreviated regions. Violin plots depict the probability density of drought ensemble (18 GCMs), and the ensemble median is shown by black cross.

The results from the exploration of the drivers of drought risk changes demonstrate that the risk changes (Figure 1) are mostly driven by shifts in the drought hazard index (DHI; Figures S2–S4 in Supporting Information S1) rather than by alterations in the composite exposure-vulnerability index (CEVI) (Figure S5 in Supporting Information S1). The spatial pattern of the drought risk changes mirrors the pattern of the changes in DHI and drought properties. We then decompose the regional changes in the drought risk into exposure-vulnerability and hazard components. A comparison between the regional changes in the DHI (Figure 2b) and CEVI (Figure 4a) with the corresponding scenarios reveals that the drivers vary with the scenario and in space. No change in CEVI is projected for 8, 6, and 9 regions under the Sustainability, Regional rivalry, and Fossil-fueled development scenarios, respectively, of which, Alaska, Australia, Greenland, north Asia, and Tibet are common among the scenarios. In the regions with no CEVI change, the drought risk change is due to the DHI change. Only in northern Europe under the Fossil-fueled development scenario,

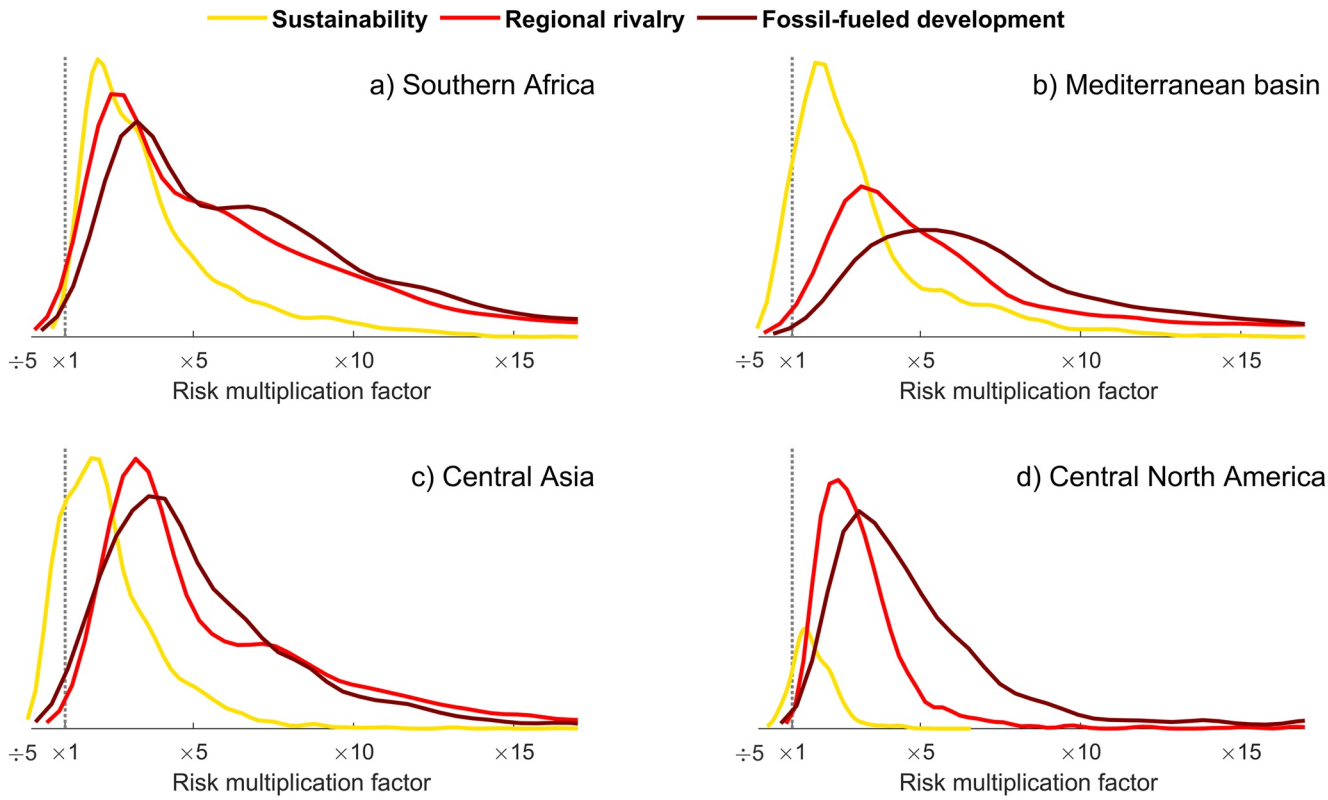

Figure 3. Distribution of drought risk changes under different scenarios for the model grid cells of hotspot regions.

no CEVI change is accompanied by no DHI change, leading to no risk change. Southeast Asia under the Sustainability and Regional rivalry scenarios and south Asia under the Fossil-fueled development scenario show an opposite pattern, where the risk change is totally attributable to the CEVI change as no change happens in DHI. The drought risk changes in 2 regions (northern Europe and western Africa) under the Sustainability scenario and in 4 regions (eastern and western Africa, eastern North America, and northern Europe) under the Regional rivalry scenario are driven by changes in both DHI and CEVI with a comparable magnitude. In 2 regions (eastern and southern Africa) under the Sustainability scenario, in 8 regions (Amazon and Mediterranean basins, central and western America, central North America, southern South America, Sahara, and southern Africa) under the Regional rivalry scenario and in 5 regions (central and western North America and eastern, southern, and western Africa) under the Fossil-fueled development scenario, the DHI increase is far larger than the CEVI increase. The drought risk change in these regions is thus more attributed to the DHI changes. In contrast, a larger increase in CEVI is observed in 2 regions (east and south Asia) under the Sustainability scenario and in one region (eastern North America) under the Fossil-fueled development scenario, attributing drought risk changes to the CEVI changes. Opposite signs of DHI and CEVI changes are seen in 6 regions (Amazon and Mediterranean basins, central North America, central America, southern South America, and central Asia) under the Sustainability scenario, in 2 regions (east and south Asia) under the Regional rivalry scenario and in 5 regions (central America, southern South America and central, east, and southeast Asia) under the Fossil-fueled development scenario, whereby the projected decrease in CEVI partially offsets the increase in DHI. The contribution of the DHI changes to the drought risk change is, therefore, larger in these regions.

We further explore the drivers of the drought risk change by analyzing the changes in the components of DHI and CEVI. The drought properties in order of decreasing magnitude of relative changes are frequency, duration, and intensity. The spatial distribution of the DHI change follows that of the drought frequency change (Figures S2–S4 in Supporting Information S1). The drought risk pattern becomes more conspicuous by a partly similar global pattern of changes in drought duration and intensity. Regionally, the drought properties hold the same order of the change magnitude in almost all regions (Figure 5). The changes in drought

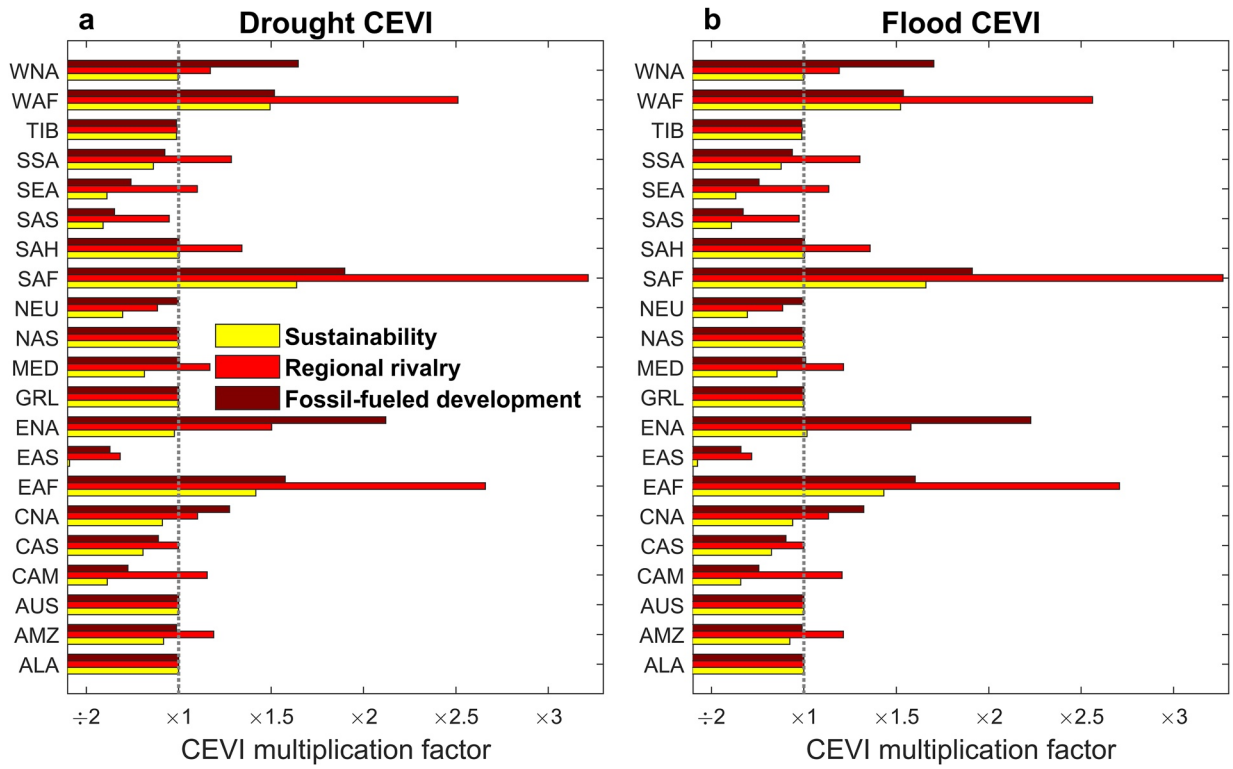

Figure 4. Change in the composite exposure-vulnerability index (CEVI) for (a) drought and (b) flood in 21 continental and subcontinental regions by 2070–2099 relative to 1971–2000. See Table S2 in Supporting Information S1 for the full names of the abbreviated regions.

frequency indeed show the most distinct regionality, with the ensemble median change ranging from −11% in northern Europe to 162% in the Sahara for the Sustainability scenario, from −23% in Greenland to 193% in the Sahara for the Regional rivalry scenario, and from −33% in Greenland to 201% in the Sahara for the Fossil-fueled development scenario (Figure 5). The regionality is also noticeable in drought duration changes, where the ensemble median change varies between −10% in Alaska and 45% in the Sahara for the Sustainability scenario, −13% in Alaska and 87% in the Mediterranean basin for the Regional rivalry scenario, and −17% in Alaska and 115% in the Mediterranean basin for the Fossil-fueled development scenario. In contrast, the spatial variation in drought intensity changes is small, ranging between −1% and 8%.

We also determine which climate variables have contributed to the drought changes. A large increase in the drought hazard in the Amazon and Mediterranean basins, Australia, central America, southern Africa, and the Sahara is due to compounding total precipitation decrease and total evapotranspiration increase (Figures S6 in Supporting Information S1). In other regions, a concomitant increase in both evapotranspiration and precipitation leads to either an increase or decrease in drought hazard. In 11 regions, the increase rate of evapotranspiration is larger than the increase rate of precipitation with the most pronounced cases in central and western North America and central Asia, again leading to a drought hazard increase. A drought hazard decrease is seen in 4 regions where the increase rate of evapotranspiration is smaller than that of precipitation.

A comparison between the spatial distributions of the drought CEVI (Figures S5 in Supporting Information S1) and its components (Figures S7–S8 in Supporting Information S1) indicates that the change in cropland proportion is the leading spatial mode of variability in the CEVI change. In fact, the high vulnerability to drought in Africa under all scenarios, in the Americas under the Regional rivalry and Fossil-fueled development scenarios, in Europe under the Fossil-fueled development scenario mainly comes from this component. High CEVI values in Africa and the Middle East are in part due to the projected population growth in the region. Thanks to a decreasing population and croplands, partly to an improving economy, the vulnerability to drought in most of Europe is low under the Sustainability scenario. In central, southern,

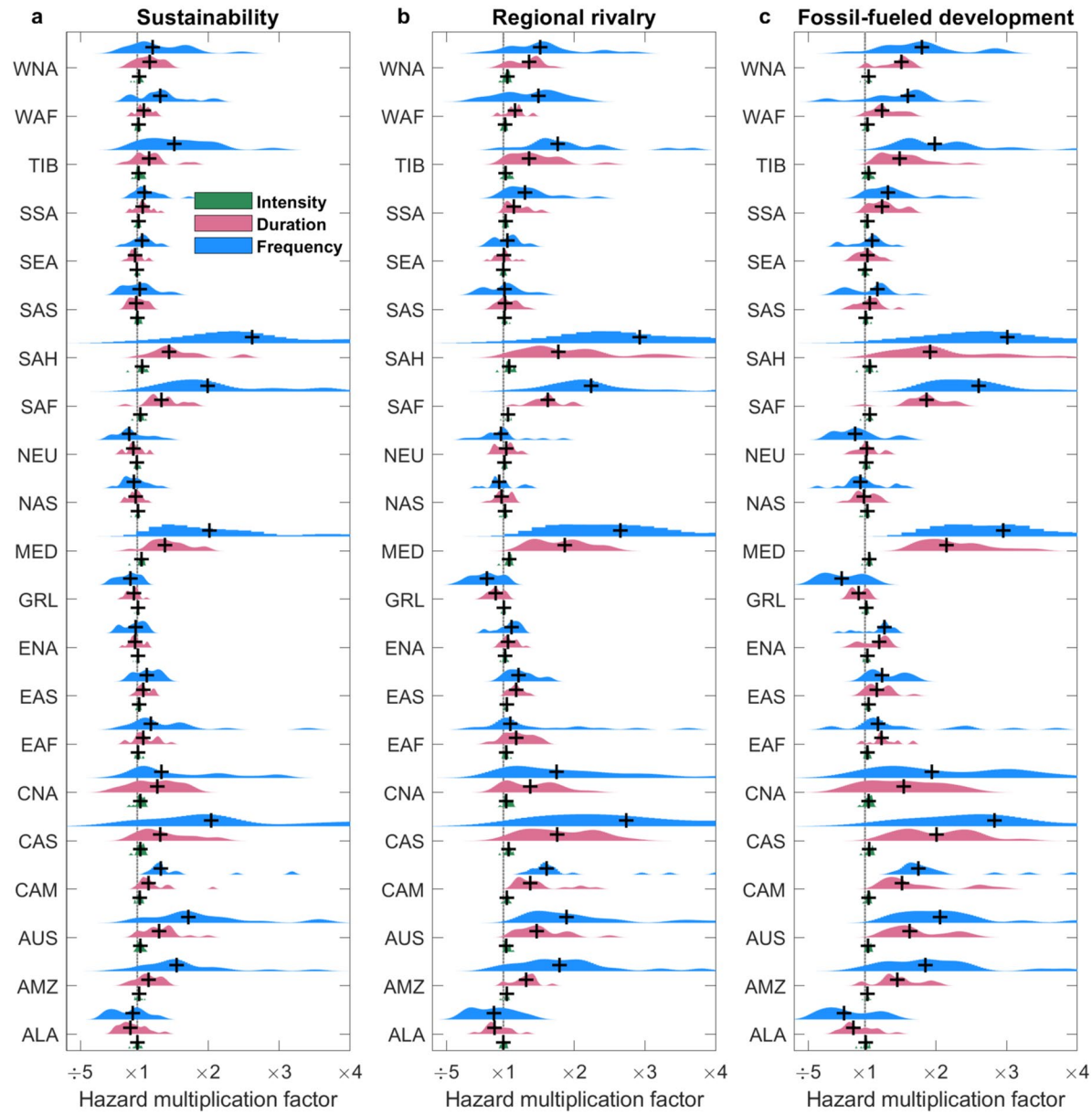

Figure 5. Change in the components of the drought hazard index (DHI) in 21 continental and subcontinental regions by 2070–2099 under the (a) Sustainability, (b) Regional rivalry and (c) Fossil-fueled development scenarios relative to 1971–2000. See Table S2 in Supporting Information S1 for the full names of the abbreviated regions. Violin plots depict the probability density of drought ensemble (18 GCMs), and the ensemble median is shown by black cross.

and eastern Asia, GDP increase and somewhat controlled population growth and cropland expansion make the CEVI value low.

3.2. Projected Changes in Flood Risk

The world map of the future flood risk changes exhibits a dramatic rise in the risk across most of the global land area (Figure 6). In contrast, the flood risk will halve mainly in central and eastern Europe and partly in Nordic countries, southern South America, and central North America. Globally, the flood risk is projected to increase by the end of the 21st century in 65%, 78%, and 78% of the analyzed landmass for the Sustainability, Regional rivalry, and Fossil-fueled development scenarios, respectively. The twofold flood risk increase is found in 33%, 56%, and 61% of the unmasked global area for the respective scenarios. For the same order

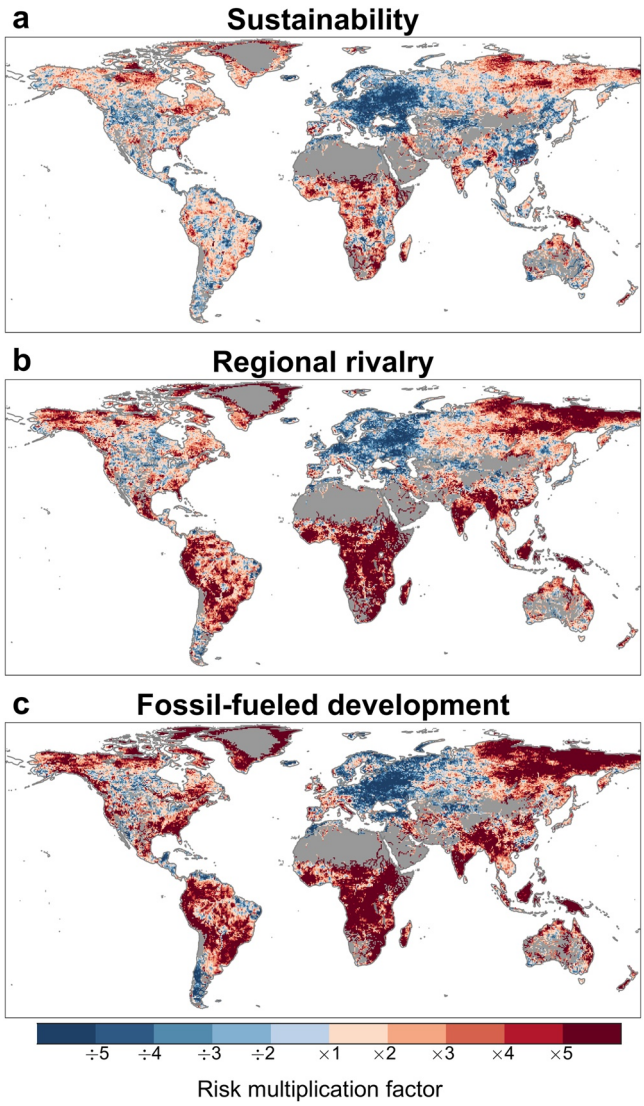

Figure 6. Global patterns of change in flood risk by 2070–2099 under (a) Sustainability, (b) Regional rivalry and (c) Fossil-fueled development scenarios relative to 1971–2000. Model grid cells with annual flow maxima of <1 $m^3 s^{-1}$ of the historical model period are screened out (gray color). The changes are based on the ensemble median of 28 experiments (7 GHMs × 4 GCMs).

of scenarios, 17%, 41%, and 79% of the area exhibit a threefold increase in the flood risk. The flood risk shows a similar order of sensitivity as the drought risk to rising GHG emissions and socioeconomic developments, highlighting the benefits of reducing GHG emissions and controlling socioeconomic changes.

The regional analysis of the change in the flood risk shows an increase in all regions except northern Europe under all scenarios, central Asia under the Sustainability and Fossil-fueled development scenarios, central America, east Asia, the Mediterranean basin, and Tibet under the Sustainability scenario (Figure 7a). Based on the ensemble median, the flood risk is likely to double at the end of the century in 4, 13, and 16 regions under the Sustainability, Regional rivalry, and Fossil-fueled development scenarios, respectively. For the respective scenarios, the flood risk is expected to triple in 0, 9, and 10 regions and to quadruple in 0, 5, and 5 regions. Eastern and southern Africa and south and southeast Asia exhibit the largest increases in the future flood risk, respectively, with at least four-fold increases for the Regional rivalry and Fossil-fueled development scenarios. Comparing the area of these regions with a quadruple flood risk increase indicates that the quadruple increase under the Fossil-fueled development scenario is observed in 79%, 69%, 65%, and 67% of the area in eastern and southern Africa and south and southeast Asia, respectively (Figure 8). For the Sustainability and Regional rivalry scenarios, the percentage area of the quadruple flood risk increase is generally smaller, ranging between 53% and 74% for the Sustainability scenario and between 17% and 28% for the Regional rivalry scenario.

The exploration of the drivers of flood risk changes shows that the flood risk changes (Figure 6) in most of the land area are generated mainly by the changes in FHI (Figures S9–S11 in Supporting Information S1) rather than the CEVI changes (Figures S5 in Supporting Information S1). In contrast, the spatial distribution of the flood risk changes follows the spatial distributions of both the FHI and CEVI changes which resemble each other. At the regional scale, however, the drivers of the flood risk change vary with region and scenario (comparing Figures 4 and 7b) as in drought risk. In 10 regions under the Fossil-fueled development scenario, the large FHI increases are muted by either a weaker increase (central and eastern North America and eastern and southern, and western Africa) or a decrease (central America, southern South America, and east, south, and southeast Asia) in CEVI. A reduction of the magnitude of the flood risk increase because of a weaker increase or decrease in CEVI compared to FHI is seen respectively in 6 and 1 regions under the Regional rivalry scenario and in 1 and 5 regions under the Sustainability scenario. In 7, 7, and 8 regions respectively under the Sustainability, Regional rivalry, and Fossil-fueled development scenarios, the flood risk change stems from the FHI change because of no CEVI change. The CEVI decrease controls the flood risk decrease in central America, central and east Asia, and the Mediterranean basin under the Sustainability scenario, and in central Asia under the Fossil-fueled development scenario. A decrease in both FHI and CEVI contributes to the flood risk decrease in northern Europe under the Sustainability and Regional rivalry scenarios. The flood risk increase in western North America under the Regional rivalry and Fossil-fueled development scenarios is driven by a CEVI increase. The CEVI contribution to the flood risk increase in 4 regions (eastern North America, Mediterranean basin, and southern and western Africa) under the Regional rivalry scenario is larger than that of FHI. The FHI and CEVI have a comparable contribution to the flood risk increase in 2 regions (southern and western Africa) under the Fossil-fueled development scenario.

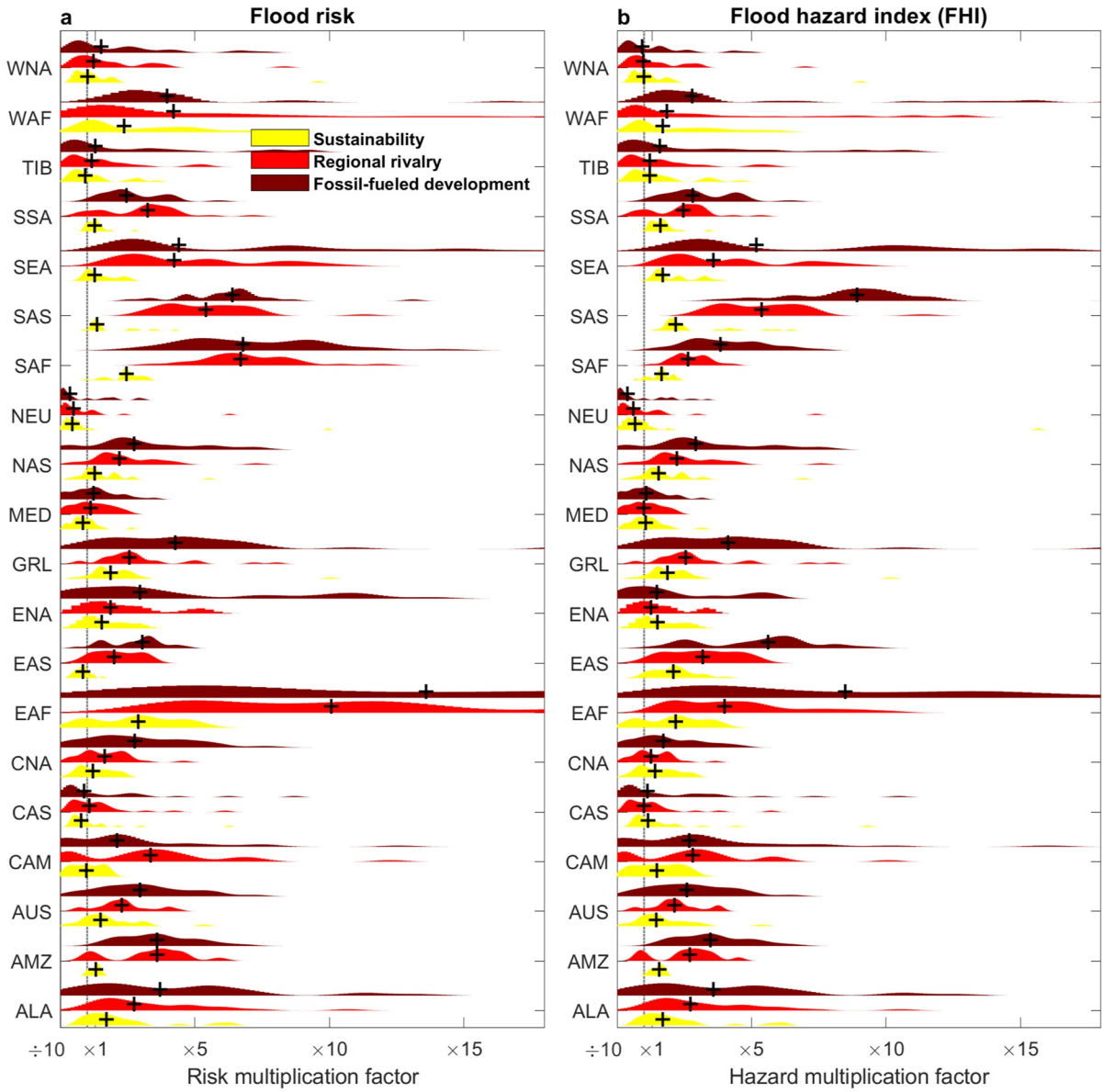

Figure 7. Change in (a) flood risk and (b) flood hazard index (FHI) in continental and subcontinental regions by 2070–2099 relative to 1971–2000. See Table S2 in Supporting Information S1 for the full names of the abbreviated regions. Model grid cells with annual flow maxima of <1 $m^3 s^{-1}$ of the historical model period are screened out, excluding the entire Sahara region. Violin plots depict the probability density of flood ensemble (28 experiments resulting from combination of 7 GHMs and 4 GCMs), and the ensemble median is shown by black cross.

The global pattern of the flood characteristics resembles each other and that of FHI (Figures S9–S11 in Supporting Information S1). The change magnitude of flood frequency is far larger than that of flood intensity. Regionally, a larger change in flood frequency than in flood intensity is seen for all regions (Figure 9), accounting for, on average, 32%, 58%, and 94% under the Sustainability, Regional rivalry, and Fossil-fueled development scenarios, respectively. The magnitude of the regional changes in flood frequency vary from −28% in northern Europe to 77% in south Asia for the Sustainability scenario, from −34% in northern Europe to 230% in south Asia for the Regional rivalry scenario, and from −55% in northern Europe to 416% in eastern Africa for the Fossil-fueled development scenario, while those for flood intensity vary from −5%, −6%, and −13 in northern Europe to 17%, 42%, and 58% in south Asia for the respective scenarios.

Comparing the spatial distributions of the flood CEVI and its components reveal that the change in cropland proportion is the largest (Figures S7–S8 in Supporting Information S1). The CEVI changes for flood

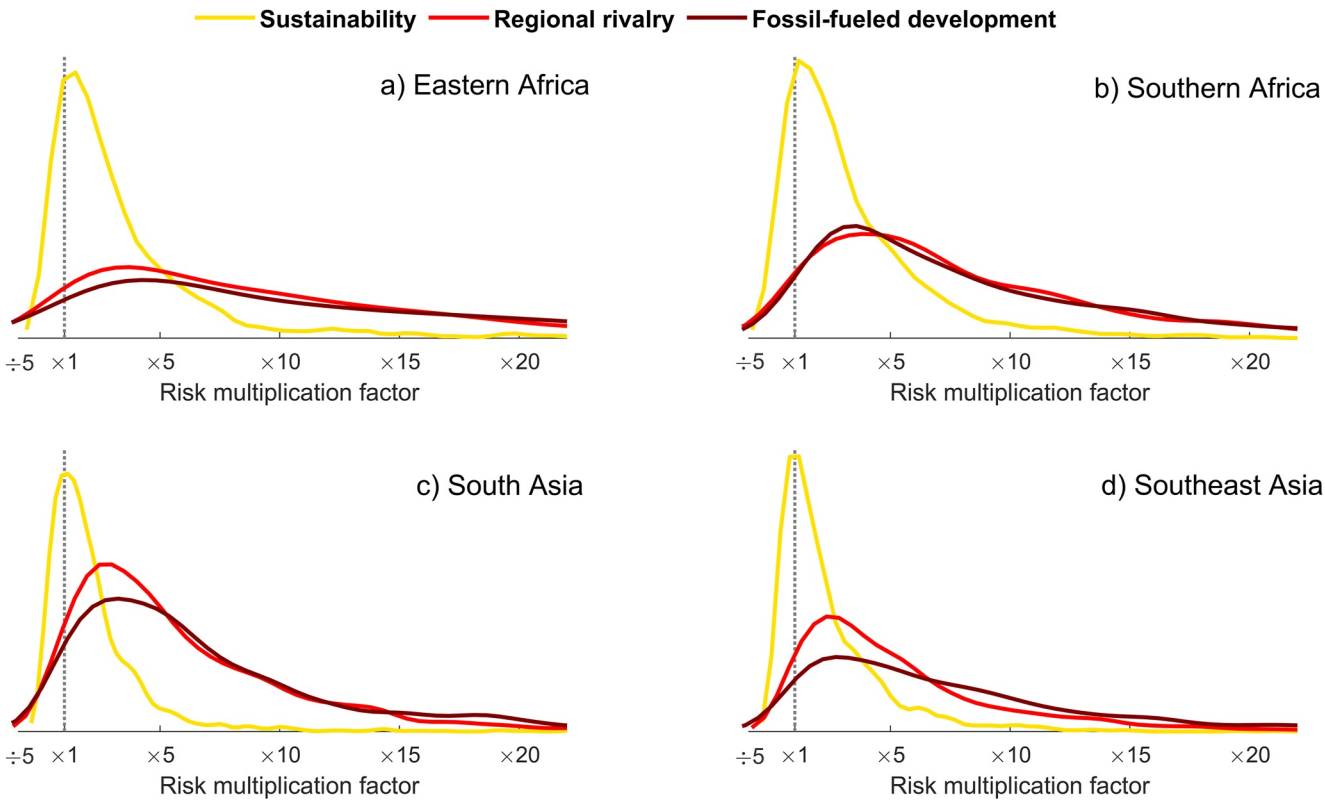

Figure 8. Distribution of flood risk changes under different scenarios for the model grid cells of hotspot regions.

and drought have an almost identical geographical pattern (Figures S6 in Supporting Information S1), making the overall impact of urbanization, which was used as an additional proxy indicator for the flood risk assessment, small. Regionally, under the Sustainability scenario, the change magnitude of the flood CEVI in 8 regions (Amazon and Mediterranean basins, central North America, central America, southern South America, and east and southeast Asia) is higher compared to the drought CEVI, while it is lower for 2 regions (northern Europe and western Africa) (Figure 4). Regionally, the change magnitude of the flood CEVI is higher compared to the drought CEVI wherever they are increasing (1, 8, and 3 regions for the Sustainability, Regional rivalry, and Fossil-fueled development scenarios, respectively) (Figure 4). The opposite situation is seen for decreasing CEVI (7, 3, and 7 regions for the Sustainability, Regional rivalry, and Fossil-fueled development scenarios, respectively): a higher decrease magnitude for the drought CEVI in comparison with the flood CEVI. In the rest of the cases, there is no change in both flood and drought CEVI or the difference between them is negligible (<5%).

3.3. Uncertainty in Drought and Flood Risk Projections

The future projections of drought and flood risk are subject to a large uncertainty (Figures S12 in Supporting Information S1). The highest total uncertainties in drought risk projections are seen in southern Africa, the Sahara, central Asia, and the Mediterranean basin, and the lowest ones in southeast Asia, south Asia, and northern Europe, and east Asia. The spatial distribution of the total uncertainty for flood risk projections is different, with the largest uncertainties in eastern, western, and southern Africa and southeast Asia, and the smallest ones in central Asia, northern Europe, and the Mediterranean basin.

The total uncertainty in the projections of future flood and drought risk is decomposed into GCM, hazard quantification method (choice between GHMs for flood and between multi-scaler indices for drought), RCP, and SSP uncertainties. For drought risk projections, hazard quantification uncertainty dominates everywhere except over southeast Asia where SSP is the main uncertainty source (Figure 10a). The hazard quantification uncertainty is larger than 50% in 12 out of the 21 regions and ranges from 24% in southeast

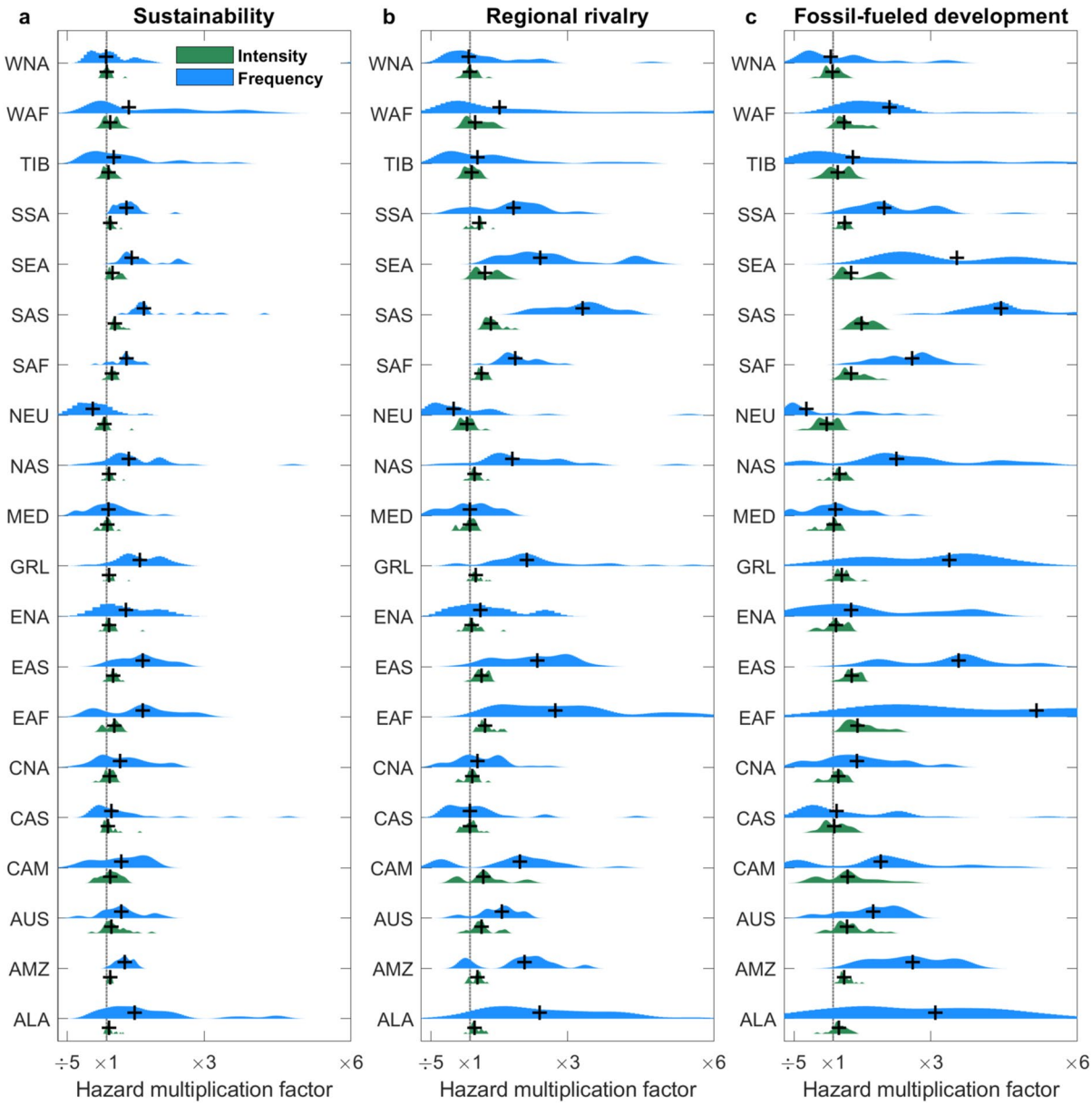

Figure 9. Change in the components of the flood hazard index (FHI) in continental and subcontinental regions by 2070–2099 under the (a) Sustainability, (b) Regional rivalry and (c) Fossil-fueled development scenarios relative to 1971–2000. See Table S2 in Supporting Information S1 for the full names of the abbreviated regions. Model grid cells with annual flow maxima of <1 $m^3 s^{-1}$ of the historical model period are screened out, excluding the entire Sahara region. Violin plots depict the probability density of flood ensemble (28 experiments resulting from combination of 7 GHMs and 4 GCMs), and the ensemble median is shown by black cross.

Asia to 67% in north Asia. In fact, the changes in the drought hazard derived from SPEI are 2, 2.8, and 3.6 times (and similar ratios for the risk) larger than those from SPI for RCP2.6, RCP6.0, and RCP8.5, respectively (Figures S13 in Supporting Information S1). It shows that the difference between SPEI- and SPI-based drought risk changes becomes more obvious under higher warming levels. A larger discrepancy between the results of different drought indices under the stronger warming of RCP8.5 is consistent with previous studies (Lehner et al., 2017). In addition to the change magnitude, an opposite sign of change (hazard decrease by SPI vs. hazard increase by SPEI) is found in 11 regions, implying that an increase in precipitation in these regions is outbalanced by an increase in atmospheric evaporative demand forced by higher temperatures. The difference between the SPI and SPEI results is statistically significant in all the regions for the three scenarios except southeast Asia under RCP2.6 (Table S2 in Supporting Information S1). The

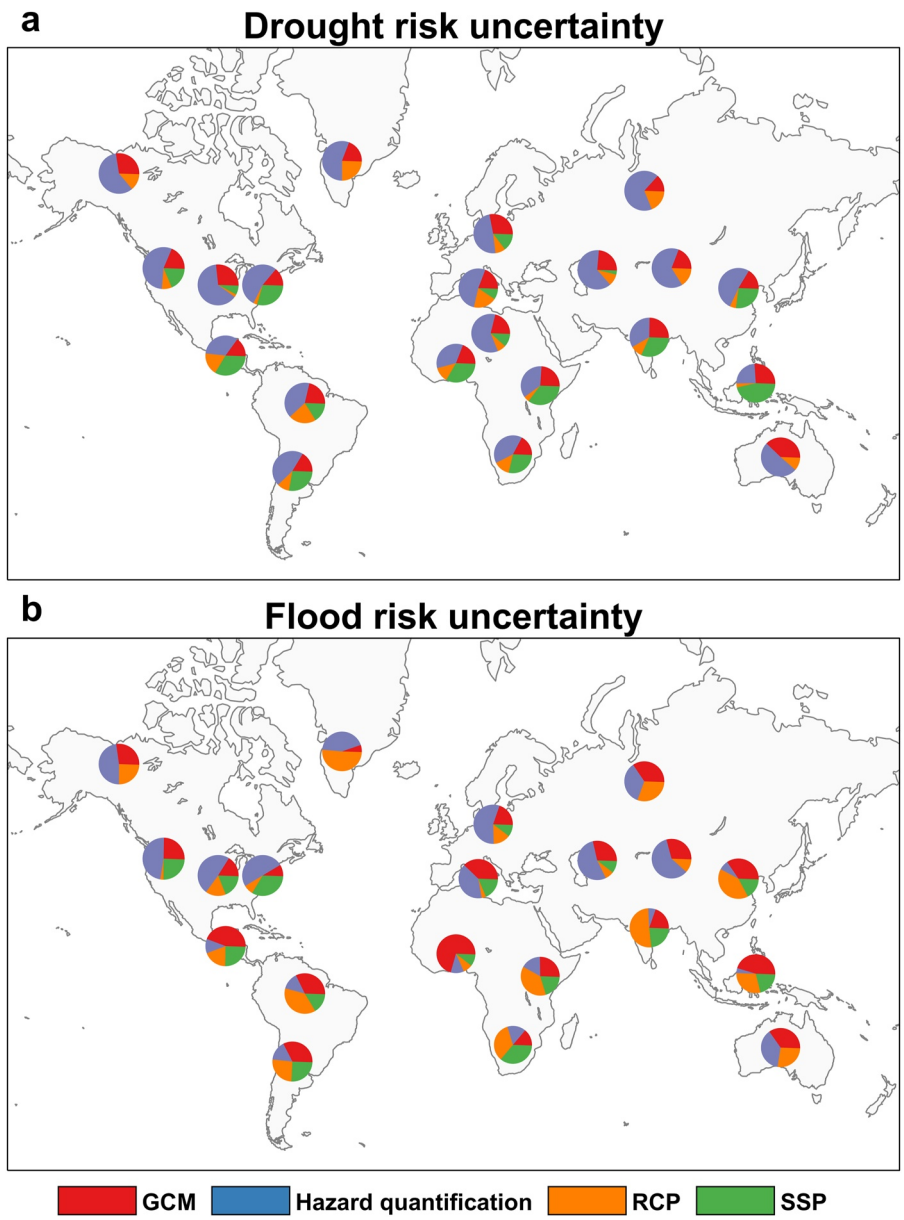

Figure 10. Fractional contribution of individual sources to total uncertainty in (a) drought and (b) flood risk changes in the continental and subcontinental regions by 2070–2099 relative to 1971–2000. RCP and SSP represent uncertainties associated to hazard and CEVI, respectively. Hazard quantification uncertainty signifies uncertainties associated to the choice of GHMs for flood quantification and of the multi-scaler indices (SPI and SPEI) for drought characterization.

uncertainty decomposition analysis also reveals that scenarios (RCP and SSP) contribute least to the total uncertainty in all regions except in central America where GCM uncertainty has the smallest contribution (Figure 10a). The contribution of GCM uncertainty ranges between 14% in north Asia and 38% in Australia.

In contrast to drought risk projections, the contribution of uncertainty sources for flood risk projections has a high spatial variability (Figure 10b). While hazard quantification dominates the total uncertainty in 9 out of the 20 considered regions for the flood analysis, it is the least important contributor in seven regions. A closer look at uncertainty decomposition of flood risk projections results reveals that hazard quantification uncertainty contributes most in the regions located in mid and high latitudes in the Northern Hemisphere (8 out of 11 regions). Overall, hazard quantification explains 4%–59% of the total variability in flood risk projections over the 20 considered regions. GCM and RCP are the most important source of uncertainty in

5 regions, with contributions of 6%–72% and 2%–51%, respectively. Only a small subset of available CMIP5 GCMs was used to force the GHMs and therefore might underestimate this source of uncertainty. SSP uncertainty is the main source in only one region, explaining 35% of the total uncertainty in southern Africa.

4. Discussion

4.1. On Drought and Flood Risk

Our results show that the drought risk increases in most of the global land area, with a decrease mainly found at high latitudes (e.g., Russia, Canada). The drought risk changes are driven by compounding changes in exposure, vulnerability, and hazard and primarily by hazard. An amplification of drought conditions in a warmer climate is anticipated owing to the theorized expectation of an increase in evaporative demand at the rate of 1.5%–4% (Scheff and Frierson, 2014) per degree warming according to the Clausius-Clapeyron relationship. This scaling rate is not, however, uniform across the globe because of the intervention of other factors such as moisture availability (Berg & McColl, 2021; Tabari, 2020). Our results also point to an increase in evaporative demand in all 21 regions of the world, confirming recent findings (Greve et al., 2019; Konapala et al., 2020). We show a more severe drought-prone condition in the future in several regions such as southern Africa and the Mediterranean basin, posing large challenges for existing socio-hydrological systems there and increasing the risk of environmental refugee displacement (Myers, 2002) and water conflicts (Hsiang et al., 2013). Based on our analysis, a larger drought increase in these regions is due to concurrent precipitation decrease and evapotranspiration increase.

We also quantified the changes in drought characteristics to understand their role in the amplified drought hazard and provide insight for adoption and mitigation strategies. As the changes in drought duration and frequency are far larger than those in drought intensity, adoption and mitigation strategies should focus more on long, frequent droughts in the future. More frequent and prolonged droughts due to climate change have also been reported using regional climate model simulations (Spinoni et al., 2020; Tabari and Willems, 2018). The increases in drought duration and frequencies would bring some complications for the disaster recovery and hydraulic system designs to withstand more prolonged and frequent periods of reduced water availabilities (Diffenbaugh et al., 2015; Naumann et al., 2018). The lengthening of drought events may also lead to more frequent megadroughts (multidecadal drought) in the future, with unprecedented stress on water resources (Ault et al., 2016).

Like the drought risk, the flood risk is also projected to increase in most of the analyzed global landmass, which for most regions stem from a flood hazard increase. The spatial pattern of flood hazard changes matches well with those shown in previous studies (Arnell & Gosling, 2016; Dankers et al., 2014; Donnelly et al., 2017; Hirabayashi et al., 2013; Lange et al., 2020). The magnitude and direction of the flood hazard change spatially vary with the role of flood generating mechanisms. The largest increases are found for the Southern Hemisphere, specifically in eastern and southern Africa and south and southeast Asia regions. Inversely, the decreasing signals are obtained in regions where flood is generated by factors other than extreme precipitation, which is generally expected to increase in the future. As an example of the regions experiencing a flood decrease, soil moisture is the dominant deriving force for flood changes over Europe, followed by snowmelt or rain-on-snow (Berghuijs et al., 2019). The flood magnitude is expected to decrease in areas with a snowmelt-dominated hydrograph in spring (Dankers et al., 2014) as precipitation shifts from snowfall to rain (Burn & Whitfield, 2016; Cunderlik and Ouarda, 2009) and the magnitude of snowmelt-related floods decreases due to a snowmelt timing change under global warming (Arnell & Gosling, 2016). An unclear direction of flood intensity changes in the regions where the most important factor is antecedence soil moisture was also noted previously and attributed to the interwoven effects of evaporation, and precipitation dynamics (Bennett et al., 2018; Ivancic and Shaw, 2015; Wasko and Nathan, 2019).

Scrutinizing flood risk results shows that in all regions except 4 (eastern and southern Africa, south and southeast Asia) under both the Regional rivalry and Fossil-fueled development scenarios and in 2 regions (Amazon basin and western Africa) under the Fossil-fueled development scenario, both increases and decreases in flood risk are projected by different GCM-GHMs combinations. It implies that the use of a single combination may lead to misleading results, calling for the use of multiple GHMs and GCMs for future flood analyses. The importance of using multiple GHMs and GCMs for analyzing and projecting extreme events

is evident from our uncertainty analysis and has been emphasized in earlier studies (Giuntoli et al., 2015; Gudmundsson et al., 2021; Hattermann et al., 2018; Hosseinzadehtalaei et al., 2020; Reinecke et al., 2021; Tabari et al., 2019). High dependence of projected precipitation changes on the used GCMs has also been found (Osuch et al., 2016; Xu et al., 2019), casting doubt on the credibility of the studies based on few and/or unrepresentative models (Wu et al., 2020).

Looking at the results of both flood and drought risk indicates that a concurrent increase in both flood and drought risk is prevalent and found in 8, 16, and 14 regions under the Sustainability, Regional rivalry, and Fossil-fueled development scenarios, respectively. Adaptation and mitigation plans will therefore be challenging in these regions, as actions implemented to diminish risk from one hazard may inadvertently result in risk increase from the other (Di Baldassarre et al., 2017). For example, drought protection favors high water storage in the reservoir, which makes dams more vulnerable to overtopping or failure when an extreme precipitation event occurs (Ward, De Ruiter, et al., 2020). The concurrent increase in both flood and drought risk is mainly the case for South America and Africa. This emphasizes the necessity for a joint analysis of drought and flood risk in these regions to develop integrated policies and practices for a deliberate and effective DRR.

4.2. On Risk Drivers

Although the risk changes in more than half of the regions are predominantly driven by the drought and flood hazard index changes especially by the hazard frequency, the exposure-vulnerability index is the controlling factor in some regions, exemplified by the high vulnerability to drought in Africa, mainly resulting from projected cropland expansion. Considering that people in these regions are highly dependent on agriculture for their livelihoods and access to food, the vulnerability to drought can be even larger than what is obtained here. For example, west Africa's severe drought period in the 1980s resulted in over half a million fatalities because of severe food shortages (Hulme, 1996; Traore et al., 2014) or north Africa's severe drought during the 2000–2011 period pushed 2–3 million people in extreme poverty (UN-DESA, 2013). Apart from the regional consequences of droughts, the global food security and cattle farming productivity will also be influenced since e.g., Brazil and Argentina in the Amazon basin and southern South America regions grow 53% of the world's soybeans and 42% of the world production of corn. While the Southern Hemisphere regions are vulnerable to natural hazards due to their insufficient infrastructural, social, and economic capacity to manage disasters, wealthy industrialized nations in the Northern Hemisphere are less vulnerable, thanks to their controlled population growth and economic prosperity.

As for the CEVI changes, the changes in flood and drought CEVI have an almost identical geographical pattern. There is also a clear resemblance between the global patterns of flood hazard and CEVI changes. This is because changes in socioeconomic elements were considered for flow simulations by most GHMs. That is to say, the historical (varying over the historical period) and present-day (fixed at 2005) socioeconomic scenarios were used respectively for historical and future discharge simulations in all the GHMs except for CLM4.5 which used the present-day scenario for both historical and future simulations. The geographical distributions of the changes in the CEVI components are comparable, as these socioeconomic factors are connected (O'Neill et al., 2014). For example, population density is linked to economic prosperity (Gu et al., 2020). The magnitude of the changes, however, notably varies among the CEVI components. This highlights the importance of using a composite exposure-vulnerability index for a comprehensive risk assessment for hydroclimatic extremes.

4.3. On Risk Uncertainty

We quantified uncertainties in future projections of flood and drought risk. The uncertainty analysis of drought risk projections specifies hazard quantification uncertainty, that is, the difference between SPEI and SPI results, as the main source. This comes as no surprise since air temperature plays a major role for a better modeling of moisture demand and availability (Ficklin and Novick, 2017; Su et al., 2018). In fact, the drought risk is underestimated using indices based on precipitation only. It was previously shown that the choice of the drought definition index greatly influences the direction and amplitude of changes (Burke & Brown, 2008). A higher sensitivity of the drought indices measuring the atmospheric demand for moisture

to temperature changes has been reported to result in large discrepancies between the outputs of these indices and SPI (Burke, 2011; Dai, 2013; Dai and Zhao, 2017; Rhee and Cho, 2016; Touma et al., 2015; Zhao and Dai, 2017) and an underestimation of megadrought probabilities (Ault et al., 2016). The big differences in projected drought risk from SPEI and SPI obtained in this study underscore the need of incorporating air temperature for drought characterization in the context of progressive warming, as otherwise the risk of future droughts may be underestimated. In other words, drought indicators based on precipitation alone cannot adequately consider the influence of warming climate (Touma et al., 2015). This finding has important mitigation implications. That is, the dependence of the drought risk on air temperature highlights the benefit of aggressive GHG emission mitigation.

The uncertainty analysis of flood risk projections, in contrast, shows a spatially varying dominance of uncertainty sources. Hazard quantification dominates the total uncertainty over Northern Hemisphere mid- and high-latitude landmass, highlighting the importance of differences in model parameterization (evapotranspiration, snow, and runoff schemes) in this region (Do et al., 2020; Haddeland et al., 2011).

5. Limitations

The simple multi-dimensional risk framework provided by our study comprehensively analyzes the risk and its contributing components of hazard, exposure, and vulnerability. It highlights the need to include all hazard characteristics rather than a single characteristic which may underestimate the overall risk. There are, however, several caveats with our analysis. The drought and flood hazard indices were developed here as a multiplication of hazard intensity, duration, and frequency. Hazard characteristics can also be integrated by means of multivariate distribution functions.

We used river flow with a 30-year return period as a proxy for flooding like Dankers et al. (2014). To calculate flood depth and inundation areas, a global river routing model with an inundation scheme such as CaMa-Flood should be employed as done by Hirabayashi et al. (2013) and Lange et al. (2020). We also quantified the flood intensity and frequency using the ISIMIP GHMs which simulate flow regimes assuming spatially consistent routing parameters within model grid cells. In that way, the real climatological and hydrological systems for a specific location may not be accurately described (Arnell & Gosling, 2016). Furthermore, the GHMs were fed by climate simulations from four GCMs out of more than 30 available CMIP5 GCMs, which were selected based on data availability and representation of equilibrium climate sensitivity (ECS) of the CMIP5 ensemble (Frieler et al., 2017). The uncertainty in the flood risk projections might therefore be biased. The coarse-scale CMIP5 GCMs have also known deficiencies in the reproduction of extreme precipitation (Freitas et al., 2020; Tripathi and Dominguez, 2013) as one of the main drivers of flood changes (Tabari, 2021), enlarging the projection uncertainty in the flood hazard and thereby the flood risk. However, developing multi-model fine-resolution long-term climate simulations on a global scale is currently not computationally feasible.

For the calculation of the composite exposure-vulnerability index (CEVI), exposure and vulnerability were assumed equally important. The relative importance of the components may, however, vary spatially. The spatial distribution of vulnerability is expected to be mainly shaped by the spatial pattern of poverty and wealth. For poor communities, a hotspot of climate vulnerability is an area with high exposure to hazards along with high population density with uneven distribution, inadequately built infrastructure, and low levels of capacity to respond to disasters. For wealthy and developed countries, it is however an exposed area as well as concentrated valuable coastal real estate, economic assets, and the high density of settlements and heavy industrialization in risk-prone areas. Furthermore, for exposure and vulnerability, we integrated four proxy indicators concerning the social, economic, and physical aspects. Other proxy indicators can also be employed to assess the social vulnerabilities regarding the awareness and capacities of communities or societies to cope with and to adapt to hazards through resilience building in socio-ecological systems. In this context, a well-informed, more educated, and motivated population toward a culture of hazard prevention, safety, and resilience can result in disaster risk reduction.

Despite these limitations, this study highlights the importance of considering the dynamic and interacting nature of hazard, exposure, and vulnerability for a holistic future risk assessment of extreme events. The framework developed in our study serves as a starting point for a more systematic risk analysis of extreme

events in future research. Such a framework provides valuable information to prioritize timely, integrated, and coordinated proactive adaptation and mitigation plans to hazards at the regional scales to prepare for changing climatic and socioeconomic conditions.

6. Conclusions

This study assessed future changes (2070–2099) in drought and flood risks at the global and regional scales, by integrating the changes in hazard characteristics and in social, economic, and physical vulnerabilities. The drought hazard was quantified by the SPEI and SPI indices using simulations of 18 CMIP5 GCMs under RCP2.6, RCP6.0, and RCP8.5 scenarios, and the flood hazard by the annual maxima using 84 ISIMIP2b realizations for the same scenarios. The drivers of drought and flood risk changes and the associated uncertainties were also analyzed. The results show a drought risk increase in most of the global landmass, with 50%, 62%, and 61% of the area experiencing an increase under the Sustainability (SSP1 & RCP2.6), Regional rivalry (SSP3 & RCP6.0), and Fossil-fueled development (SSP5 & RCP8.5) scenarios, respectively. The amplitude of changes in the drought risk is not uniform and varies among the regions. The highest drought risk increase of about five-fold is found for southern Africa, the Mediterranean basin, central Asia, and central North America. A similar spatial and scenario dependence is found for flood risk changes. The flood risk is projected to increase in the vast majority of the global land area (33%–61% depending on scenario), with the largest increases in eastern and southern Africa and south and southeast Asia regions. The global hotspot regions of concurrent, large drought and flood risk increase are identified in South America and Africa, where local governments should be prepared to deal with the challenges to develop informed, integrated climate policies and practices for deliberate and effective disaster risk reduction.

The drivers of drought and flood risk changes demonstrate a distinct regionality, but in more than half of the regions, the risk changes are predominantly driven by the drought and flood hazard index changes especially by the hazard frequency. Nevertheless, the exposure-vulnerability index changes control the risk changes in some regions, exemplified by the high vulnerability to drought in Africa, primarily originating from a projected cropland expansion. The decomposition of uncertainty sources for drought risk changes reveals hazard quantification methods as the main source everywhere. For flood risk changes, the role of uncertainty contributors varies spatially, but with the dominance of hazard quantification source over Northern Hemisphere mid- and high-latitude landmass.

Data Availability Statement

The ISIMIP and socioeconomic data used in this study can be accessed from https://esg.pik-potsdam.de/search/isimip/ and the CMIP5 data from https://esgf-node.llnl.gov/search/cmip5/. The land use data are available at https://www-iam.nies.go.jp/aim/data_tools/aimssp/aimssp.html.

Acknowledgments
The CMIP5, ISIMIP and socioeconomic data providers are acknowledged. Hossein Tabari thanks the Research Foundation–Flanders (FWO) for financial support (grant number: 12P3219N). Parisa Hosseinzadehtalaei appreciates KU Leuven for a postdoctoral mandate (PDM/20/084).

References

Ahmadalipour, A., Moradkhani, H., Castelletti, A., & Magliocca, N. (2019). Future drought risk in Africa: Integrating vulnerability, climate change, and population growth. *Science of the Total Environment*, *662*, 672–686. https://doi.org/10.1016/j.scitotenv.2019.01.278

Alborzi, A., Mirchi, A., Moftakhari, H., Mallakpour, I., Alian, S., Nazemi, A., et al. (2018). Climate-informed environmental inflows to revive a drying lake facing meteorological and anthropogenic droughts. *Environmental Research Letters*, *13*(8), 084010. https://doi.org/10.1088/1748-9326/aad246

Alfieri, L., Bisselink, B., Dottori, F., Naumann, G., de Roo, A., Salamon, P., et al. (2017). Global projections of river flood risk in a warmer world. *Earth's Future*, *5*, 171–182. https://doi.org/10.1002/2016ef000485

Alfieri, L., Feyen, L., & Di Baldassarre, G. (2016). Increasing flood risk under climate change: A pan-European assessment of the benefits of four adaptation strategies. *Climatic Change*, *136*, 507–521. https://doi.org/10.1007/s10584-016-1641-1

Andrijevic, M., Cuaresma, J. C., Muttarak, R., & Schleussner, C. F. (2020). Governance in socioeconomic pathways and its role for future adaptive capacity. *Nature Sustainability*, *3*(1), 35–41. https://doi.org/10.1038/s41893-019-0405-0

Arnell, N. W., & Gosling, S. N. (2016). The impacts of climate change on river flood risk at the global scale. *Climatic Change*, *134*(3), 387–401. https://doi.org/10.1007/s10584-014-1084-5

Arnell, N. W., Lowe, J. A., Lloyd-Hughes, B., & Osborn, T. J. (2018). The impacts avoided with a 1.5°C climate target: A global and regional assessment. *Climatic Change*, *147*, 61–76. https://doi.org/10.1007/s10584-017-2115-9

Ault, T. R., Mankin, J. S., Cook, B. I., & Smerdon, J. E. (2016). Relative impacts of mitigation, temperature, and precipitation on 21st-century megadrought risk in the American Southwest. *Science Advances*, *2*(10), e1600873. https://doi.org/10.1126/sciadv.1600873

Bennett, B., Leonard, M., Deng, Y., & Westra, S. (2018). An empirical investigation into the effect of antecedent precipitation on flood volume. *Journal of Hydrology*, *567*, 435–445. https://doi.org/10.1016/j.jhydrol.2018.10.025

Berg, A., & McColl, K. A. (2021). No projected global drylands expansion under greenhouse warming. *Nature Climate Change*, *11*, 331–337. https://doi.org/10.1038/s41558-021-01007-8

Berghuijs, W. R., Harrigan, S., Molnar, P., Slater, L. J., & Kirchner, J. W. (2019). The relative importance of different flood-generating mechanisms across Europe. *Water Resources Research*, *55*(6), 4582–4593. https://doi.org/10.1029/2019wr024841

Best, M. J., Pryor, M., Clark, D. B., Rooney, G. G., Essery, R. L. H., Ménard, C. B., et al. (2011). The Joint UK Land Environment Simulator (JULES), model description–Part 1: Energy and water fluxes. *Geoscientific Model Development*, *4*(3), 677–699. https://doi.org/10.5194/gmd-4-677-2011

Blauhut, V., Stahl, K., Stagge, J. H., Tallaksen, L. M., Stefano, L. D., & Vogt, J. (2016). Estimating drought risk across Europe from reported drought impacts, drought indices, and vulnerability factors. *Hydrology and Earth System Sciences*, *20*(7), 2779–2800. https://doi.org/10.5194/hess-20-2779-2016

Bondeau, A., Smith, P. C., Zaehle, S., Schaphoff, S., Lucht, W., Cramer, W., et al. (2007). Modelling the role of agriculture for the 20th century global terrestrial carbon balance. *Global Change Biology*, *13*, 679–706. https://doi.org/10.1111/j.1365-2486.2006.01305.x

Burke, E. J. (2011). Understanding the sensitivity of different drought metrics to the drivers of drought under increased atmospheric CO2. *Journal of Hydrometeorology*, *12*(6), 1378–1394. https://doi.org/10.1175/2011jhm1386.1

Burke, E. J., & Brown, S. J. (2008). Evaluating uncertainties in the projection of future drought. *Journal of Hydrometeorology*, *9*(2), 292–299. https://doi.org/10.1175/2007jhm929.1

Burn, D. H., & Whitfield, P. H. (2016). Changes in floods and flood regimes in Canada. *Canadian Water Resources Journal*, *41*, 139–150. https://doi.org/10.1080/07011784.2015.1026844

Cardona, O. D., van Aalst, M. K., Birkmann, O. D., Fordham, M., McGregor, G., Perez, R., et al. (2012). Determinants of risk: Exposure and vulnerability. In C. B. Field, V. Barros, T. F. Stocker, D. Qin, D. J. Dokken, K. L. Ebi, M. D. Mastrandrea, K. J. Mach, G.-K. Plattner, S. K. Allen, M. Tignor, & P. M. Midgley (Eds.), *Managing the risks of extreme events and disasters to advance climate change adaptation. A special report of working groups I and II of the intergovernmental panel on climate change (IPCC)* (pp. 65–108): Cambridge University Press.

Carrão, H., Naumann, G., & Barbosa, P. (2016). Mapping global patterns of drought risk: An empirical framework based on sub-national estimates of hazard, exposure and vulnerability. *Global Environmental Change*, *39*, 108–124. https://doi.org/10.1016/j.gloenvcha.2016.04.012

Chiang, F., Mazdiyasni, O., & AghaKouchak, A. (2018). Amplified warming of droughts in southern United States in observations and model simulations. *Science Advances*, *4*(8), eaat2380. https://doi.org/10.1126/sciadv.aat2380

CRED. (2015). *The human cost of natural disasters: A global perspective*: Centre for Research on the Epidemiology of Disasters (CRED).

Cunderlik, J. M., & Ouarda, T. B. M. J. (2009). Trends in the timing and magnitude of floods in Canada. *Journal of Hydrology*, *375*, 471–480. https://doi.org/10.1016/j.jhydrol.2009.06.050

Dai, A. (2013). Increasing drought under global warming in observations and models. *Nature Climate Change*, *3*(1), 52–58. https://doi.org/10.1038/nclimate1633

Dai, A., & Zhao, T. (2017). Uncertainties in historical changes and future projections of drought. Part I: Estimates of historical drought changes. *Climatic Change*, *144*(3), 519–533. https://doi.org/10.1007/s10584-016-1705-2

Dankers, R., Arnell, N. W., Clark, D. B., Falloon, P. D., Fekete, B. M., Gosling, S. N., et al. (2014). First look at changes in flood hazard in the Inter-Sectoral Impact Model Intercomparison Project ensemble. *Proceedings of the National Academy of Sciences*, *111*(9), 3257–3261. https://doi.org/10.1073/pnas.1302078110

Di Baldassarre, G., Martinez, F., Kalantari, Z., & Viglione, A. (2017). Drought and flood in the Anthropocene: Feedback mechanisms in reservoir operation. *Earth System Dynamics*, *8*(1), 225–233. https://doi.org/10.5194/esd-8-225-2017

Diaconescu, E. P., Gachon, P., & Laprise, R. (2015). On the remapping procedure of daily precipitation statistics and indices used in regional climate model evaluation. *Journal of Hydrometeorology*, *16*(6), 2301–2310. https://doi.org/10.1175/jhm-d-15-0025.1

Diffenbaugh, N. S., Swain, D. L., & Touma, D. (2015). Anthropogenic warming has increased drought risk in California. *Proceedings of the National Academy of Sciences*, *112*(13), 3931–3936. https://doi.org/10.1073/pnas.1422385112

Do, H. X., Zhao, F., Westra, S., Leonard, M., Gudmundsson, L., Boulange, J. E. S., et al. (2020). Historical and future changes in global flood magnitude–evidence from a model–observation investigation. *Hydrology and Earth System Sciences*, *24*(3), 1543–1564. https://doi.org/10.5194/hess-24-1543-2020

Donnelly, C., Greuell, W., Andersson, J., Gerten, D., Pisacane, G., Roudier, P., & Ludwig, F. (2017). Impacts of climate change on European hydrology at 1.5, 2 and 3 degrees mean global warming above preindustrial level. *Climatic Change*, *143*, 13–26. https://doi.org/10.1007/s10584-017-1971-7

Dottori, F., Szewczyk, W., Ciscar, J.-C., Zhao, F., Alfieri, L., Hirabayashi, Y., et al. (2018). Increased human and economic losses from river flooding with anthropogenic warming. *Nature Climate Change*, *8*(9), 781–786. https://doi.org/10.1038/s41558-018-0257-z

Engström, J., Jafarzadegan, K., & Moradkhani, H. (2020). Drought Vulnerability in the United States: An Integrated Assessment. *Water*, *12*, 2033. https://doi.org/10.3390/w12072033

Farahmand, A., & AghaKouchak, A. (2015). A generalized framework for deriving nonparametric standardized drought indicators. *Advances in Water Resources*, *76*, 140–145. https://doi.org/10.1016/j.advwatres.2014.11.012

Ficklin, D. L., & Novick, K. A. (2017). Historic and projected changes in vapor pressure deficit suggest a continental-scale drying of the United States atmosphere. *Journal of Geophysical Research: Atmospheres*, *122*, 2061–2079. https://doi.org/10.1002/2016jd025855

Formetta, G., & Feyen, L. (2019). Empirical evidence of declining global vulnerability to climate-related hazards. *Global Environmental Change*, *57*, 101920. https://doi.org/10.1016/j.gloenvcha.2019.05.004

Freitas, S. R., Putman, W. M., Arnold, N. P., Adams, D. K., & Grell, G. A. (2020). Cascading toward a kilometer-scale GCM: Impacts of a scale-aware convection parameterization in the Goddard earth observing system GCM. *Geophysical Research Letters*, *47*(17), e2020GL087682. https://doi.org/10.1029/2020gl087682

Frieler, K., Lange, S., Piontek, F., Reyer, C. P. O., Schewe, J., Warszawski, L., et al. (2017). Assessing the impacts of 1.5°C global warming—Simulation protocol of the Inter-Sectoral Impact Model Intercomparison Project (ISIMIP2b). *Geoscientific Model Development*, *10*(12), 4321–4345. https://doi.org/10.5194/gmd-10-4321-2017

Fujimori, S., Hasegawa, T., Ito, A., Takahashi, K., & Masui, T. (2018). Gridded emissions and land-use data for 2005–2100 under diverse socioeconomic and climate mitigation scenarios. *Scientific Data*, *5*, 180210. https://doi.org/10.1038/sdata.2018.210

Giorgi, F., & Francisco, R. (2000). Uncertainties in regional climate change prediction: A regional analysis of ensemble simulations with the HADCM2 coupled AOGCM. *Climate Dynamics*, *16*(2–3), 169–182. https://doi.org/10.1007/pl00013733

Giuntoli, I., Vidal, J. P., Prudhomme, C., & Hannah, D. M. (2015). Future hydrological extremes: The uncertainty from multiple global climate and global hydrological models. *Earth System Dynamics*, *6*, 267–285. https://doi.org/10.5194/esd-6-267-2015

Greve, P., Kahil, T., Mochizuki, J., Schinko, T., Satoh, Y., Burek, P., et al. (2018). Global assessment of water challenges under uncertainty in water scarcity projections. *Nature Sustainability*, *1*(9), 486–494. https://doi.org/10.1038/s41893-018-0134-9

Greve, P., Roderick, M. L., Ukkola, A. M., & Wada, Y. (2019). The aridity index under global warming. *Environmental Research Letters*, *14*(12), 124006. https://doi.org/10.1088/1748-9326/ab5046

Gu, L., Chen, J., Yin, J., Sullivan, S. C., Wang, H.-M., Guo, S., et al. (2020). Projected increases in magnitude and socioeconomic exposure of global droughts in 1.5 and 2°C warmer climates. *Hydrology and Earth System Sciences*, *24*(1), 451–472. https://doi.org/10.5194/hess-24-451-2020

Gudmundsson, L., Boulange, J., Do, H. X., Gosling, S. N., Grillakis, M. G., Koutroulis, A. G., et al. (2021). Globally observed trends in mean and extreme river flow attributed to climate change. *Science*, *371*, 1159–1162. https://doi.org/10.1126/science.aba3996

Guimberteau, M., Ducharne, A., Ciais, P., Boisier, J. P., Peng, S., De Weirdt, M., & Verbeeck, H. (2014). Testing conceptual and physically based soil hydrology schemes against observations for the Amazon Basin. *Geoscientific Model Development*, *7*(3), 1115–1136. https://doi.org/10.5194/gmd-7-1115-2014

Haddeland, I., Clark, D. B., Franssen, W., Ludwig, F., Voß, F., Arnell, N. W., et al. (2011). Multimodel estimate of the global terrestrial water balance: Setup and first results. *Journal of Hydrometeorology*, *12*(5), 869–884. https://doi.org/10.1175/2011jhm1324.1

Hanasaki, N., Kanae, S., Oki, T., Masuda, K., Motoya, K., Shirakawa, N., et al. (2008). An integrated model for the assessment of global water resources—Part 1: Model description and input meteorological forcing. *Hydrology and Earth System Sciences*, *12*, 1007–1025. https://doi.org/10.5194/hess-12-1007-2008

Hargreaves, G. H., & Samani, Z. A. (1985). Reference crop evapotranspiration from temperature. *Applied Engineering in Agriculture*, *1*(2), 96–99. https://doi.org/10.13031/2013.26773

Hattermann, F. F., Vetter, T., Breuer, L., Su, B., Daggupati, P., Donnelly, C., et al. (2018). Sources of uncertainty in hydrological climate impact assessment: A cross-scale study. *Environmental Research Letters*, *13*(1), 015006. https://doi.org/10.1088/1748-9326/aa9938

Hinkel, J., Lincke, D., Vafeidis, A. T., Perrette, M., Nicholls, R. J., Tol, R. S. J., et al. (2014). Coastal flood damage and adaptation costs under 21st century sea-level rise. *Proceedings of the National Academy of Sciences*, *111*(9), 3292–3297. https://doi.org/10.1073/pnas.1222469111

Hirabayashi, Y., Mahendran, R., Koirala, S., Konoshima, L., Yamazaki, D., Watanabe, S., et al. (2013). Global flood risk under climate change. *Nature Climate Change*, *3*(9), 816–821. https://doi.org/10.1038/nclimate1911

Hirschi, M., Seneviratne, S. I., Alexandrov, V., Boberg, F., Boroneant, C., Christensen, O. B., et al. (2011). Observational evidence for soil-moisture impact on hot extremes in southeastern Europe. *Nature Geoscience*, *4*(1), 17–21. https://doi.org/10.1038/ngeo1032

Hosseinzadehtalaei, P., Tabari, H., & Willems, P. (2017). Uncertainty assessment for climate change impact on intense precipitation: How many model runs do we need? *International Journal of Climatology*, *37*, 1105–1117. https://doi.org/10.1002/joc.5069

Hosseinzadehtalaei, P., Tabari, H., & Willems, P. (2020). Satellite-based data driven quantification of pluvial floods over Europe under future climatic and socioeconomic changes. *Science of the Total Environment*, *15*, 137688. https://doi.org/10.1016/j.scitotenv.2020.137688

Hsiang, S. M., Burke, M., & Miguel, E. (2013). Quantifying the influence of climate on human conflict. *Science*, *341*(6151), 1235367–1235367. https://doi.org/10.1126/science.1235367

Hulme, M. (1996). Recent climatic change in the world's drylands. *Geophysical Research Letters*, *23*(1), 61–64. https://doi.org/10.1029/95gl03586

IPCC. (2013). Summary for policymakers. Climate Change. In T. F. Stocker, D. Qin, G. K. Plattner, M. Tignor, S. Allen, J. KBoschung, A. Nauels, Y. Xia, V. Bex, & P. M. Midgley (Eds.), *The physical science basis, contribution of working group I to the fifth assessment report of the intergovernmental panel on climate change*.

Ivancic, T., & Shaw, S. (2015). Examining why trends in very heavy precipitation should not be mistaken for trends in very high river discharge. *Climatic Change*, *133*, 681–693. https://doi.org/10.1007/s10584-015-1476-1

Jongman, B., Ward, P. J., & Aerts, J. C. J. H. (2012). Global exposure to river and coastal flooding: Long term trends and changes. *Global Environmental Change*, *22*(4), 823–835. https://doi.org/10.1016/j.gloenvcha.2012.07.004

Jongman, B., Winsemius, H. C., Aerts, J. C., de Perez, E. C., van Aalst, M. K., Kron, W., & Ward, P. J. (2015). Declining vulnerability to river floods and the global benefits of adaptation. *Proceedings of the National Academy of Sciences*, *112*(18), E2271–E2280. https://doi.org/10.1073/pnas.1414439112

Kam, P. M., Aznar-Siguan, G., Schewe, J., Milano, L., Ginnetti, J., Willner, S., et al. (2021). Global warming and population change both heighten future risk of human displacement due to river floods. *Environmental Research Letters*, *16*(4), 044026. https://doi.org/10.1088/1748-9326/abd26c

Khajehei, S., Ahmadalipour, A., Shao, W., & Moradkhani, H. (2020). A place-based assessment of flash flood hazard and vulnerability in the contiguous United States. *Scientific Reports*, *10*(1), 1–12. https://doi.org/10.1038/s41598-019-57349-z

Kim, H., Park, J., Yoo, J., & Kim, T.-W. (2015). Assessment of drought hazard, vulnerability, and risk: A case study for administrative districts in South Korea. *Journal of Hydro-environment Research*, *9*, 28–35. https://doi.org/10.1016/j.jher.2013.07.003

Kinoshita, Y., Tanoue, M., Watanabe, S., & Hirabayashi, Y. (2018). Quantifying the effect of autonomous adaptation to global river flood projections: Application to future flood risk assessments. *Environmental Research Letters*, *13*(1), 014006. https://doi.org/10.1088/1748-9326/aa9401

Klein Goldewijk, K., Beusen, A., Doelman, J., & Stehfest, E. (2017). Anthropogenic land use estimates for the Holocene–HYDE 3.2. *Earth System Science Data*, *9*, 927–953. https://doi.org/10.5194/essd-9-927-2017

Knorr, W., Arneth, A., & Jiang, L. (2016). Demographic controls of future global fire risk. *Nature Climate Change*, *6*(8), 781–785. https://doi.org/10.1038/nclimate2999

Konapala, G., Mishra, A. K., Wada, Y., & Mann, M. E. (2020). Climate change will affect global water availability through compounding changes in seasonal precipitation and evaporation. *Nature Communications*, *11*, 3044. https://doi.org/10.1038/s41467-020-16757-w

Lange, S., Volkholz, J., Geiger, T., Zhao, F., Vega, I., Veldkamp, T., et al. (2020). Projecting exposure to extreme climate impact events across six event categories and three spatial scales. *Earth's Future*, *8*, e2020EF001616. https://doi.org/10.1029/2020ef001616

Lawrence, D. M., Oleson, K. W., Flanner, M. G., Thornton, P. E., Swenson, S. C., Lawrence, P. J., et al. (2011). Parameterization improvements and functional and structural advances in version 4 of the Community Land Model. *Journal of Advances in Modeling Earth Systems*, *3*, 27. Art. M03001. https://doi.org/10.1029/2011ms00045

Lehner, F., Coats, S., Stocker, T. F., Pendergrass, A. G., Sanderson, B. M., Raible, C. C., & Smerdon, J. E. (2017). Projected drought risk in 1.5C and 2C warmer climates. *Geophysical Research Letters*, *44*(14), 7419–7428. https://doi.org/10.1002/2017gl074117

Li, Y., Ye, W., Wang, M., & Yan, X. (2009). Climate change and drought: A risk assessment of crop-yield impacts. *Climate Research*, *39*, 31–46. https://doi.org/10.3354/cr00797

Liao, X., Xu, W., Zhang, J., Li, Y., & Tian, Y. (2019). Global exposure to rainstorms and the contribution rates of climate change and population change. *Science of the Total Environment*, *663*, 644–653. https://doi.org/10.1016/j.scitotenv.2019.01.290

Liu, W., Sun, F., Lim, W. H., Zhang, J., Wang, H., Shiogama, H., & Zhang, Y. (2018). Global drought and severe drought-affected populations in 1.5 and 2°C warmer worlds. *Earth System Dynamics*, *9*(1), 267–283. https://doi.org/10.5194/esd-9-267-2018

Maccioni, P., Kossida, M., Brocca, L., & Moramarco, T. (2015). Assessment of the drought hazard in the Tiber River basin in central Italy and a comparison of new and commonly used meteorological indicators. *Journal of Hydrologic Engineering*, *20*(8), 05014029. https://doi.org/10.1061/(asce)he.1943-5584.0001094

McKee, T. B., Doesken, N. J., & Kleist, J. (1993). The relationship of drought frequency and duration to time scales. In. Proc. Eighth Conf. On Applied Climatology (pp. 179–183): Amer. Meteor. Soc.

Meza, I., Siebert, S., Döll, P., Kusche, J., Herbert, C., Eyshi Rezaei, E., et al. (2020). Global-scale drought risk assessment for agricultural systems. *Natural Hazards and Earth System Sciences*, *20*(2), 695–712. https://doi.org/10.5194/nhess-20-695-2020

Mueller Schmied, H., Adam, L., Eisner, S., Fink, G., Florken, M., Kim, H., et al. (2016). Variations of global and continental water balance components as impacted by climate forcing uncertainty and human water use. *Hydrology and Earth System Sciences*, *20*(7), 2877–2898.

Murakami, D., & Yamagata, Y. (2019). Estimation of gridded population and GDP scenarios with spatially explicit statistical downscaling. *Sustainability*, *11*(7), 2106. https://doi.org/10.3390/su11072106

Myers, N. (2002). Environmental refugees: A growing phenomenon of the 21st century. *Philosophical Transactions of the Royal Society B: Biological Sciences*, *357*(1420), 609–613. https://doi.org/10.1098/rstb.2001.0953

Nasiri, H., Mohd Yusof, M. J., & Mohammad Ali, T. A. (2016). An overview to flood vulnerability assessment methods. *Sustainable Water Resources Management*, *2*, 331–336. https://doi.org/10.1007/s40899-016-0051-x

Naumann, G., Alfieri, L., Wyser, K., Mentaschi, L., Betts, R. A., Carrao, H., et al. (2018). Global changes in drought conditions under different levels of warming. *Geophysical Research Letters*, *45*(7), 3285–3296. https://doi.org/10.1002/2017gl076521

NDMC. (2018). *SPIGenerator software link*: University of Nebraska-Lincoln. Retrieved from https://drought.unl.edu/droughtmonitoring/SPI/SPIProgram.aspx

O'Neill, B. C., Kriegler, E., Riahi, K., Ebi, K. L., Hallegatte, S., et al. (2014). A new scenario framework for climate change research: The concept of shared socioeconomic pathways. *Climatic Change*, *122*(3), 387–400.

O'Neill, B. C., Tebaldi, C., van Vuuren, D. P., Eyring, V., Friedlingstein, P., Hurtt, G., et al. (2016). The scenario model intercomparison project (ScenarioMIP) for CMIP6. *Geoscientific Model Development*, *9*(9), 3461–3482. https://doi.org/10.5194/gmd-9-3461-2016

Osuch, M., Romanowicz, R. J., Lawrence, D., & Wong, W. K. (2016). Trends in projections of standardized precipitation indices in a future climate in Poland. *Hydrology and Earth System Sciences*, *20*(5), 1947–1969. https://doi.org/10.5194/hess-20-1947-2016

Peña-Gallardo, M., Vicente-Serrano, S. M., Domínguez-Castro, F., & Beguería, S. (2019). The impact of drought on the productivity of two rainfed crops in Spain. *Natural Hazards and Earth System Sciences*, *19*(6), 215–1234. https://doi.org/10.5194/nhess-19-1215-2019

Pokhrel, Y., Felfelani, F., Satoh, Y., Boulange, J., Burek, P., Gädeke, A., et al. (2021). Global terrestrial water storage and drought severity under climate change. *Nature Climate Change*, *11*, 226–233. https://doi.org/10.1038/s41558-020-00972-w

Popp, A., Humpenöder, F., Weindl, I., Bodirsky, B. L., Bonsch, M., Lotze-Campen, H., et al. (2014). Land-use protection for climate change mitigation. *Nature Climate Change*, *4*, 1095–1098. https://doi.org/10.1038/nclimate2444

Reinecke, R., Müller Schmied, H., Trautmann, T., Andersen, L. S., Burek, P., Flörke, M., et al. (2021). Uncertainty of simulated groundwater recharge at different global warming levels: A global-scale multi-model ensemble study. *Hydrology and Earth System Sciences*, *25*, 787–810. https://doi.org/10.5194/hess-25-787-2021

Rhee, J., & Cho, J. (2016). Future changes in drought characteristics: Regional analysis for South Korea under CMIP5 projections. *Journal of Hydrometeorology*, *17*(1), 437–451. https://doi.org/10.1175/jhm-d-15-0027.1

Samir, K. C., & Lutz, W. (2014). Demographic scenarios by age, sex and education corresponding to the SSP narratives. *Population and Environment*, *35*(3), 243–260.

Scheff, J., & Frierson, D. M. (2014). Scaling potential evapotranspiration with greenhouse warming. *Journal of Climate*, *27*, 1539–1558. https://doi.org/10.1175/jcli-d-13-00233.1

Scheuer, S., Haase, D., & Meyer, V. (2011). Exploring multicriteria flood vulnerability by integrating economic, social and ecological dimensions of flood risk and coping capacity: From a starting point view towards an end point view of vulnerability. *Natural Hazards*, *58*, 731–751. https://doi.org/10.1007/s11069-010-9666-7

Sheffield, J., & Wood, E. F. (2011). *Drought: Past problems and future scenarios*. Earthscan Publications Ltd.

Smirnov, O., Zhang, M., Xiao, T., Orbell, J., Lobben, A., & Gordon, J. (2016). The relative importance of climate change and population growth for exposure to future extreme droughts. *Climatic Change*, *138*, 41–53. https://doi.org/10.1007/s10584-016-1716-z

Spinoni, J., Barbosa, P., Bucchignani, E., Cassano, J., Cavazos, T., Christensen, J. H., et al. (2020). Future global meteorological drought hot spots: A study based on CORDEX Data. *Journal of Climate*, *33*(9), 3635–3661. https://doi.org/10.1175/jcli-d-19-0084.1

Stevanovic, M., Popp, A., Lotze-Campen, H., Dietrich, J. P., Müller, C., Bonsch, M., et al. (2016). High-end climate change impacts on agricultural welfare. *Science Advances*, *2*(8), e1501452.

Su, B., Huang, J., Fischer, T., Wang, Y., Kundzewicz, Z. W., Zhai, J., et al. (2018). Drought losses in China might double between the 1.5C and 2.0C warming. *Proceedings of the National Academy of Sciences*, *115*(42), 10600–10605. https://doi.org/10.1073/pnas.1802129115

Tabari, H. (2020). Climate change impact on flood and extreme precipitation increases with water availability. *Scientific Reports*, *10*(1), 1–10. https://doi.org/10.1038/s41598-020-70816-2

Tabari, H. (2021). Extreme value analysis dilemma for climate change impact assessment on global flood and extreme precipitation. *Journal of Hydrology*, *593*, 125932. https://doi.org/10.1016/j.jhydrol.2020.125932

Tabari, H., Abghari, H., & Hosseinzadeh Talaee, P. (2012). Temporal trends and spatial characteristics of drought and rainfall in arid and semiarid regions of Iran. *Hydrological Processes*, *26*(22), 3351–3361. https://doi.org/10.1002/hyp.8460

Tabari, H., Hosseinzadehtalaei, P., AghaKouchak, A., & Willems, P. (2019). Latitudinal heterogeneity and hotspots of uncertainty in projected extreme precipitation. *Environmental Research Letters*, *14*(12), 124032. https://doi.org/10.1088/1748-9326/ab55fd

Tabari, H., & Willems, P. (2018). More prolonged droughts by the end of the century in the Middle East. *Environmental Research Letters*, *13*(10), 104005. https://doi.org/10.1088/1748-9326/aae09c

Takata, K., Emori, S., & Watanabe, T. (2003). Development of the minimal advanced treatments of surface interaction and runoff. *Global and Planetary Change*, *38*, 209–222. https://doi.org/10.1016/s0921-8181(03)00030-4

Tanoue, M., Hirabayashi, Y., & Ikeuchi, H. (2016). Global-scale river flood vulnerability in the last 50 years. *Scientific Reports*, *6*(1), 1–9. https://doi.org/10.1038/srep36021

Taylor, K. E., Stouffer, R. J., & Meehl, G. A. (2012). An overview of CMIP5 and the experiment design. *Bulletin of the American Meteorological Society*, *93*, 485–498. https://doi.org/10.1175/bams-d-11-00094.1

Telteu, C. E., Müller Schmied, H., Thiery, W., Leng, G., Burek, P., Liu, X., et al. (2021). Understanding each other's models: A standard representation of global water models to support improvement, intercomparison, and communication. *Geoscientific Model Development*, *14*, 3843–3878. https://doi.org/10.5194/gmd-14-3843-2021

Thiery, W., Davin, E. L., Lawrence, D. M., Hirsch, A. L., Hauser, M., & Seneviratne, S. I. (2017). Present-day irrigation mitigates heat extremes. *Journal of Geophysical Research: Atmospheres*, *122*(3), 1403–1422. https://doi.org/10.1002/2016jd025740

Touma, D., Ashfaq, M., Nayak, M. A., Kao, S. C., & Diffenbaugh, N. S. (2015). A multi-model and multi-index evaluation of drought characteristics in the 21st century. *Journal of Hydrology*, *526*, 196–207. https://doi.org/10.1016/j.jhydrol.2014.12.011

Traore, S. B., Ali, A., Tinni, S. H., Samake, M., Garba, I., Maigari, I., et al. (2014). AGRHYMET: A drought monitoring and capacity building center in the West Africa Region. *Weather and Climate Extremes*, *3*, 22–30. https://doi.org/10.1016/j.wace.2014.03.008

Tripathi, O. P., & Dominguez, F. (2013). Effects of spatial resolution in the simulation of daily and subdaily precipitation in the southwestern US. *Journal of Geophysical Research: Atmospheres*, *118*(14), 7591–7605. https://doi.org/10.1002/jgrd.50590

UN-DESA. (2013). *Establishing drought early warning systems in west Asia and North Africa. Technical report*: United Nations Department of Economic and Social Affairs.

UNFCCC. (2013). *Decision 2/CP. 19 Warsaw international mechanism for loss and damage associated with climate change impacts*. FCCC/CP/2013/10/Add.1, available at: http://unfccc.int/resource/docs/2013/cop19/eng/10a01.pdf

UNISDR. (2013). *Global assessment report on disaster risk reduction 2013. From share risk to shared value*: The Business case for Disaster Risk Reduction.

UNISDR. (2015). *Sendai framework for disaster risk reduction 2015–2030, united nations international strategy for disaster reduction*. Available at: https://unisdr.org/we/inform/publications/43291

Vafeidis, A. T., Schuerch, M., Wolff, C., Spencer, T., Merkens, J. L., Hinkel, J., et al. (2019). Water-level attenuation in global-scale assessments of exposure to coastal flooding: A sensitivity analysis. *Natural Hazards and Earth System Sciences*, *19*(5), 973–984. https://doi.org/10.5194/nhess-19-973-2019

Van Vuuren, D. P., Edmonds, J., Kainuma, M., Riahi, K., Thomson, A, Hibbard, K., et al. (2011). The representative concentration pathways: An overview. *Climatic Change*, *109*(1), 5–31. https://doi.org/10.1007/s10584-011-0148-z

Vicente-Serrano, S. M., Beguería, S., & López-Moreno, J. I. (2010). A multiscalar drought index sensitive to global warming: The standardized precipitation evapotranspiration index. *Journal of Climate*, *23*(7), 1696–1718. https://doi.org/10.1175/2009jcli2909.1

Vousdoukas, M. I., Mentaschi, L., Hinkel, J., Ward, P. J., Mongelli, I., Ciscar, J. C., & Feyen, L. (2020). Economic motivation for raising coastal flood defenses in Europe. *Nature Communications*, *11*(1), 1–11. https://doi.org/10.1038/s41467-020-15665-3

Vousdoukas, M. I., Mentaschi, L., Voukouvalas, E., Bianchi, A., Dottori, F., & Feyen, L. (2018). Climatic and socioeconomic controls of future coastal flood risk in Europe. *Nature Climate Change*, *8*(9), 776–780. https://doi.org/10.1038/s41558-018-0260-4

Ward, P. J., Blauhut, V., Bloemendaal, N., Daniell, E. J., De Ruiter, P. J., Duncan, J. M., et al. (2020). Natural hazard risk assessments at the global scale. *Natural Hazards and Earth System Sciences*, *20*, 1069–1096. https://doi.org/10.5194/nhess-20-1069-2020

Ward, P. J., De Ruiter, M. C., De Mard, J., Schroter, K., Loon, A. V., Veldkamp, T., et al. (2020). The need to integrate flood and drought disaster risk reduction strategies. *Water Security*, *11*, 100070. https://doi.org/10.1016/j.wasec.2020.100070

Ward, P. J., Jongman, B., Aerts, J. C. J. H., Bates, P. D., Botzen, W. J. W., Diaz Loaiza, A., et al. (2017). A global framework for future costs and benefits of river-flood protection in urban areas. *Nature Climate Change*, *7*, 642–646. https://doi.org/10.1038/nclimate3350

Ward, P. J., Jongman, B., Weiland, F. S., Bouwman, A., van Beek, R., Bierkens, M. F. P., et al. (2013). Assessing flood risk at the global scale: Model setup, results, and sensitivity. *Environmental Research Letters*, *8*(4), 044019. https://doi.org/10.1088/1748-9326/8/4/044019

Wasko, C., & Nathan, R. (2019). Influence of changes in rainfall and soil moisture on trends in flooding. *Journal of Hydrology*, *575*, 432–441. https://doi.org/10.1016/j.jhydrol.2019.05.054

Webster, M., Forest, C., Reilly, J., Babiker, M., Kicklighter, D., Mayer, M., et al. (2003). Uncertainty analysis of climate change and policy response. *Climatic Change*, *61*(3), 295–320. https://doi.org/10.1023/b:clim.0000004564.09961.9f

Willner, S. N., Levermann, A., Zhao, F., & Frieler, K. (2018). Adaptation required to preserve future high-end river flood risk at present levels. *Science Advances*, *4*(1), eaao1914. https://doi.org/10.1126/sciadv.aao1914

Winsemius, H. C., Aerts, J. C. J. H., van Beek, L. P. H., Bierkens, M. F. P., Bouwman, A., Jongman, B., et al. (2016). Global drivers of future river flood risk. *Nature Climate Change*, *6*, 381–385. https://doi.org/10.1038/nclimate2893

Winsemius, H. C., Van Beek, L. P. H., Jongman, B., Ward, P. J., & Bouwman, A. (2013). A framework for global river flood risk assessments. *Hydrology and Earth System Sciences*, *17*, 1871–1892. https://doi.org/10.5194/hess-17-1871-2013

WMO: World Meteorological Organization. (2012). *Standardized precipitation index user guide (svoboda M, Hayes M, Wood D)*: WMO-No. 1090.

Wu, C., Yeh, P. J. F., Chen, Y. Y., Hu, B. X., & Huang, G. (2020). Future Precipitation-Driven Meteorological Drought Changes in the CMIP5 Multimodel Ensembles under 1.5° C and 2°C Global Warming. *Journal of Hydrometeorology*, *21*(9), 2177–2196. https://doi.org/10.1175/jhm-d-19-0299.1

Wu, H., Hayes, M. J., Wilhite, D. A., & Svoboda, M. D. (2005). The effect of the length of record on the standardized precipitation index calculation. *International Journal of Climatology*, *25*, 505–520. https://doi.org/10.1002/joc.1142

Xu, K., Xu, B., Ju, J., Wu, C., Dai, H., & Hu, B. X. (2019). Projection and uncertainty of precipitation extremes in the CMIP5 multimodel ensembles over nine major basins in China. *Atmospheric Research*, *226*, 122–137. https://doi.org/10.1016/j.atmosres.2019.04.018

Zhao, T., & Dai, A. (2017). Uncertainties in historical changes and future projections of drought. Part II: Model-simulated historical and future drought changes. *Climatic Change*, *144*(3), 535–548. https://doi.org/10.1007/s10584-016-1742-x